Title

Bone-marrow macrophage-derived GPNMB protein binds to orphan receptor GPR39 and plays a critical role in cardiac repair

Journal

Nature Cardiovascular Research, 3(11)

ISSN

2731-0590

Authors

Ramadoss, Sivakumar
Qin, Juan
Tao, Bo
et al.

Publication Date

2024-11-01

DOI

10.1038/s44161-024-00555-4

Peer reviewed

nature cardiovascular research

Article

https://doi.org/10.1038/s44161-024-00555-4

Bone-marrow macrophage-derived GPNMB protein binds to orphan receptor GPR39 and plays a critical role in cardiac repair

Received: 14 September 2023

Accepted: 26 September 2024

Published online: 25 October 2024

Check for updates

Sivakumar Ramadoss[1,2,3,4,5,6,12], Juan Qin[1,2,3,4,5,6,12], Bo Tao[1,2,3,4,5,6], Nathan E. Thomas[7,8], Edward Cao[1,2,3,4,5,6], Rimao Wu[1,2,3,4,5,6], Daniel R. Sandoval[7], Ann Piermatteo[7], Kaare V. Grunddal[7], Feiyang Ma[9], Shen Li[1,2,3,4,5,6], Baiming Sun[1,2,3,4,5,6], Yonggang Zhou[1,2,3,4,5,6], Jijun Wan[1,2,3,4,5,6], Matteo Pellegrini[3,4,5,6], Birgitte Holst[10], Aldons J. Lusis[1,11], Philip L.S.M. Gordts[7,8] & Arjun Deb[1,2,3,4,5,6]

Glycoprotein nonmetastatic melanoma protein B (GPNMB) is a type I transmembrane protein initially identified in nonmetastatic melanomas and has been associated with human heart failure; however, its role in cardiac injury and function remains unclear. Here we show that GPNMB expression is elevated in failing human and mouse hearts after myocardial infarction (MI). Lineage tracing and bone-marrow transplantation reveal that bone-marrow-derived macrophages are the main source of GPNMB in injured hearts. Using genetic loss-of-function models, we demonstrate that GPNMB deficiency leads to increased mortality, cardiac rupture and rapid post-MI left ventricular dysfunction. Conversely, increasing circulating GPNMB levels through viral delivery improves heart function after MI. Single-cell transcriptomics show that GPNMB enhances myocyte contraction and reduces fibroblast activation. Additionally, we identified GPR39 as a receptor for circulating GPNMB, with its absence negating the beneficial effects. These findings highlight a pivotal role of macrophage-derived GPNMBs in post-MI cardiac repair through GPR39 signaling.

The mammalian heart does not regenerate robustly after myocardial infarction (MI) and heals itself via a fibrotic repair response. A complex sequence of spatiotemporally defined cellular events regulate the cardiac repair response after cardiac injury and determines post-MI heart function[1]. Myocardial necrosis results in an initial recruitment of neutrophils that is replaced within a few days by a monocyte–macrophage infiltrate. Macrophages secrete a slew of cytokines and growth factors that initiate fibroblast and endothelial cell proliferation and play a critical role in formation of granulation tissue[2]. The injured cardiac tissue thus forms a niche within the organ where different types of cell populations respond to each other via secreted signals. Paracrine communication between different cell populations in the infarcted heart affects key repair processes such as inflammation, myocyte hypertrophy, fibrosis and angiogenesis and is considered to be an attractive target for augmenting post-MI heart function[3,4].

Glycoprotein nonmetastatic melanoma protein B (GPNMB) was first identified as a gene expressed in a melanoma cell line with low metastatic potential[5] but since then it has been observed to be expressed in a wide variety of cells, including osteoblasts, dendritic cells, macrophages, melanocytes and microglia[6]. GPNMB is a highly glycosylated single-pass type I transmembrane protein and the extracellular domain of GPNMB (GPNMB-ECD) can be cleaved by the ADAM group of proteases to form

A full list of affiliations appears at the end of the paper. e-mail: adeb@mednet.ucla.edu

an extracellular ligand with biological effects[7]. GPNMB is thought to play a role in cancer progression and regulation of adaptive and innate immunity[8]. GPNMB expression increases in multiple organs after acute injury where it is thought to modulate wound repair[9–11]. For instance, following bone fractures, GPNMB accelerates fracture healing and bone formation[12]. GPNMB expression increases in the heart in rodent models of myocardial injury[13] and in human population studies, individuals with heart failure had lower circulating GPNMB levels than control individuals without any heart failure[14]. These observations suggest a role for GPNMB in regulating post-infarction outcomes but the mechanisms of GPNMB effects on the infarcted heart remain unclear.

In this report, we investigate the role of GPNMB in regulating cardiac repair after MI. We first analyzed human population datasets and observed significantly upregulated expression of GPNMB in the hearts of individuals with ischemic cardiomyopathy. After MI, GPNMB levels significantly increased in infarcted murine hearts and using bone-marrow transplantation and lineage-tracing studies, we showed that bone-marrow macrophages are the predominant source of GPNMB expression in the infarcted heart. Using genetic loss and gain-of-function approaches, we demonstrate that GPNMB exerts pleiotropic effects on cell populations in the infarcted heart and plays a pivotal role in regulating myocyte cyto-protection and cardiac repair. Using chemical crosslinking and immunoprecipitation studies, we identify the orphan receptor GPR39, as a receptor for GPNMB-ECD and demonstrate that GPNMB mediates its physiological effects, in part, through GPR39.

Results

GPNMB is expressed in the failing human heart and infarcted murine hearts

We first analyzed a large gene expression dataset of humans with cardiomyopathy where left ventricular (LV) genome-wide gene expression was determined in failing hearts collected at transplantation and compared to healthy donor controls[15,16]. We observed that GPNMB expression in hearts from individuals with ischemic cardiomyopathy was significantly higher than in control hearts (Fig. 1a). We next subjected 8–12-week-old mice (C57BL/6 background) to MI by permanent ligation of the left anterior descending coronary artery that supplies blood flow to the LV myocardium[17]. Hearts were collected at 3, 7, 14 and 21 days after cardiac injury and tissue from the injured region and remote to the area of injury were subjected to qPCR to determine temporal changes in GPNMB expression. We observed that GPNMB gene expression in the injured region increased by orders of magnitude compared to the uninjured region and its expression peaked at 7 days after injury (Fig. 1b). Western blotting of the infarcted region demonstrated a significant increase in the known glycosylated isoforms of GPNMB (Fig. 1c,d). To determine the identity of the cell expressing GPNMB in the infarcted heart, we performed immunostaining with a panoply of myocyte and nonmyocyte markers and observed that GPNMB was expressed by cells of the monocyte–macrophage lineage. GPNMB-positive cells expressed the pan-hematopoietic marker CD45 and coexpressed monocyte–macrophage markers, including CD68, CD11b and F4/80 (Fig. 1e); however, GPNMB-expressing cells in the infarcted region did not express markers of other cell types, including cardiomyocytes, fibroblasts, endothelial cells and pericytes (Fig. 1e,f and Extended Data Fig. 1a). To confirm the findings on immunostaining, we collected the heart at day 7 post-injury and dissociated the cells, performed flow cytometry and confirmed that the majority of GPNMB-expressing cells coexpressed monocyte–macrophage markers, $CD45^+/CD68^+/CD11b^+$/Ly6c in the infarcted heart (Extended Data Fig. 1b). We next analyzed single-cell transcriptomics data of murine hearts at 7 days after infarction[18] and observed GPNMB to be predominantly expressed by macrophages (Fig. 1g,h) and not by other nonmyocyte cell population, corroborating our findings on immunostaining.

Bone-marrow-derived cells are the principal source of GPNMB expression in the infarcted heart

We next determined whether the bone marrow is the principal source of monocytes/macrophages that express GPNMB in the infarcted heart. To demonstrate this, we transplanted bone marrow from CD45.2-DsRed mice into co-syngeneic CD45.1 recipient mice (Fig. 2a). Eight weeks following transplantation, we observed that the number of circulating DsRed cells constituted 97% of all circulating mononuclear cells in the peripheral blood demonstrating successful engraftment of CD45.2 marrow into CD45.1 mice (Fig. 2b). We next subjected the recipient chimeric CD45.1 mice to MI and collected the heart at 7 days after injury when GPNMB expression peaks. On immunofluorescent staining, we observed that 99% of GPNMB-expressing cells in the infarcted heart coexpressed the bone-marrow reporter DsRed thus demonstrating the bone marrow to be an exclusive source of GPNMB in the infarcted heart (Fig. 2c,d). Flow cytometry on the infarcted heart of CD45.1 mice transplanted with CD45.2-DsRed bone marrow again confirmed more than 94% of GPNMB-expressing cells to coexpress the DsRed fluorophore (Fig. 2e). These findings, taken together, demonstrate that bone-marrow mononuclear cells that are recruited to the heart following MI are the principal source of GPNMB in the infarcted heart. To further confirm the origin of the GPNMB-expressing cell population in the injured heart, we performed genetic-labeling experiments using the dual reporter mice $Ccr2^{RFP}Cx3cr1^{GFP}$ that express red fluorescent protein (RFP) in $Ccr2^+$ myeloid cells or monocytes and green fluorescent protein (GFP) in Cx3cr1-expressing monocytes/macrophages[19]. We subjected these animals to MI and collected their hearts at day 7 after injury to isolate nonmyocyte cells for flow cytometry analysis. We observed that the fraction of $GPNMB^+$ cells in the injured heart were of myeloid lineage with 63 ± 10% expressing GFP ($Cx3Cr1^+$) and 24 ± 6% expressing RFP ($Ccr2^+$) (Extended Data Fig. 2a,b). Although the genetic labeling is not permanent here, these experiments corroborate the findings of the bone-marrow transplantation experiments and demonstrate the myeloid cell source of GPNMB-expressing cells in the injured heart.

Fig. 1 | GPNMB expression is upregulated in humans with ischemic cardiomyopathy and in murine hearts after MI. a, Analysis of GPNMB gene expression in human failing hearts compared to nonfailing control hearts. GPNMB expression values from the Gene Expression Omnibus dataset (GSE57338) were compared using an unpaired Welch's *t*-test. Box boundaries are the 25th and 75th percentiles of the data; whiskers extend to at most 1.5 × interquartile range (IQR) (75th percentile to 25th percentile). Residuals for ischemic hearts ranged from −1.65 to 1.61 and residuals for nonfailing hearts ranged from −1.53 to 0.84. **b**, qPCR demonstrating temporal expression of GPNMB in the infarcted murine hearts versus uninjured remote region (mean ± s.e.m., $n = 5$ animals per group and time point; $^*P < 0.038$, $^{**}P < 0.006$; two-tailed Student's *t*-test). **c**, Representative western blot showing expression of GPNMB in the injured versus remote area of mice heart on day 7 after MI. The bands show glycosylated form of GPNMB precursor (~97 kDa) and mature (~116 kDa) proteins (each lane represents an independent animal, $n = 3$ per group). **d**, Densitometric quantification of western blot demonstrating fold change GPNMB level (mean ± s.e.m., $n = 3$ independent animals, $^*P < 0.0263$, two-tailed Student's *t*-test). **e**, Immunofluorescent staining and confocal microscopy of GPNMB expression in uninjured and injured regions of heart demonstrating that GPNMB (green, arrowheads) is strongly coexpressed with CD45, CD68, CD11b and F4/80 markers (red, arrowheads) but not coexpressed with troponin at day 7 post-MI (representative images, $n = 3$). **f**, Fraction of GPNMB-expressing cells that coexpress different cell markers in injured region (GPNMB is not expressed by fibroblasts (CD90.2), endothelial cells (CD31), pericytes (CD146, NG2) and cardiomyocytes (troponin)) ($n = 3$ animals). **g**, Analysis of single-cell transcriptomics of the injured heart at 7 days demonstrating expression of GPNMB in various cell populations ($n = 3$ animals). **h**, Violin plot of the single-cell RNA-seq of nonmyocytes isolated from the injured heart at 7 days demonstrating GPNMB expression across various nonmyocyte populations ($n = 3$ animals). DAPI, 4,6-diamidino-2-phenylindole. All data represented as mean ± s.e.m.

https://doi.org/10.1038/s44161-024-00555-4

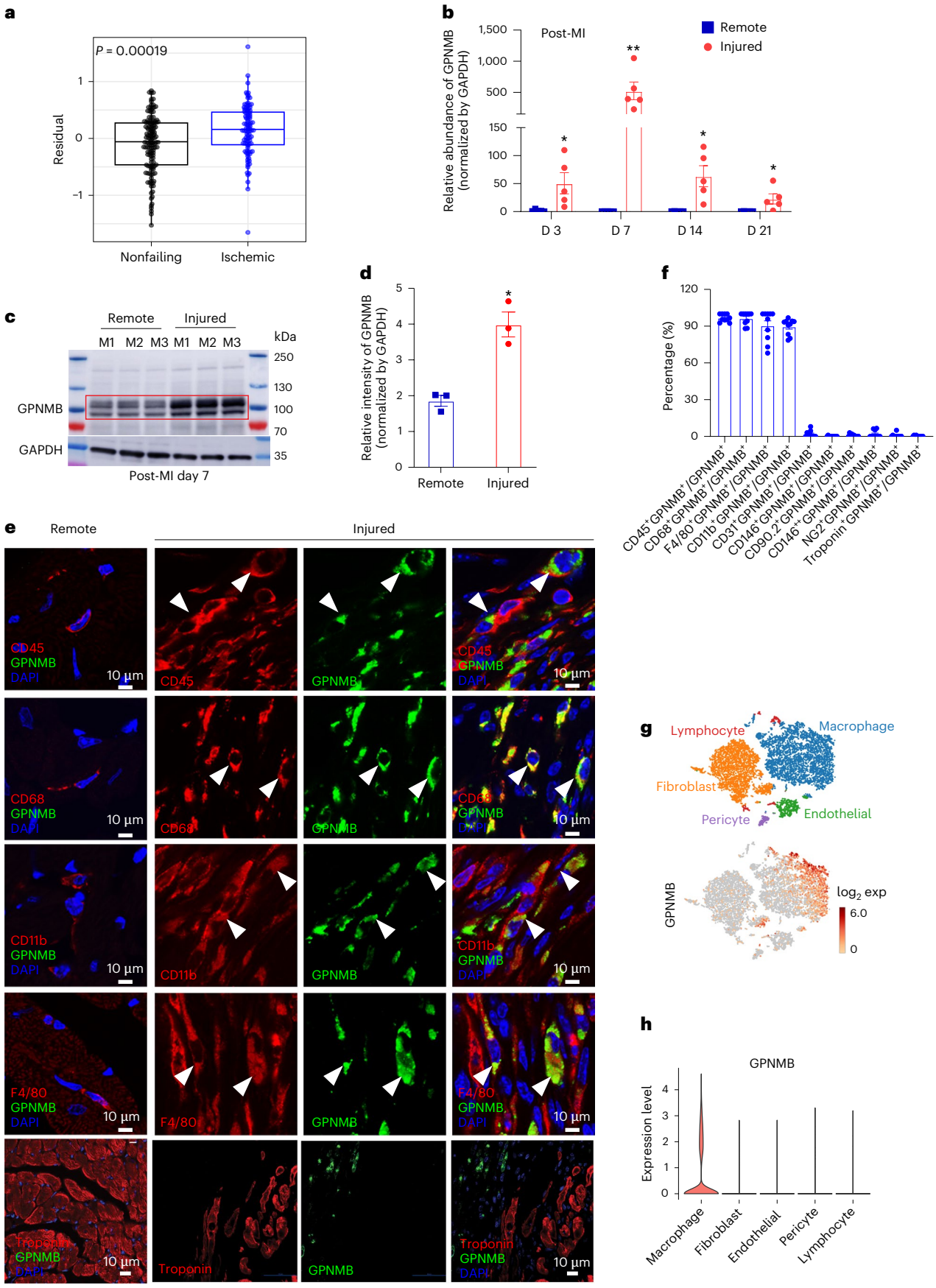

https://doi.org/10.1038/s44161-024-00555-4

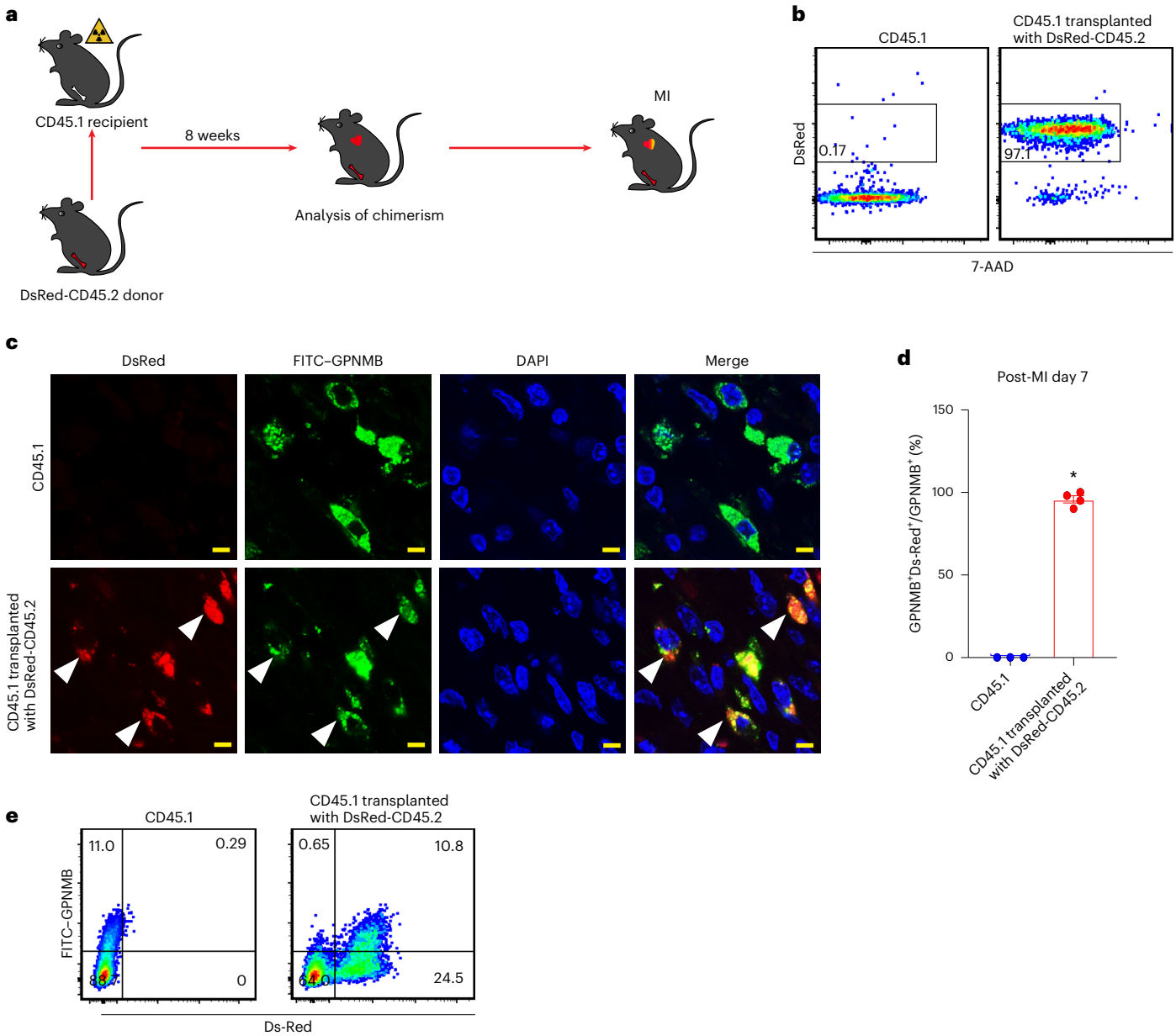

Fig. 2 | Bone-marrow-derived cells recruited to the infarcted heart are the source of GPNMB. a, Schematic illustration of bone-marrow transplantation. CD45.1 male recipients were irradiated and transplanted with the bone marrow from DsRed CD45.2 male donors. Engraftment (chimerism) analysis was carried out after 8 weeks and animals were subjected to MI at 9 weeks following transplantation ($n = 10$ recipients and $n = 2$ donors). **b**, Analysis of chimerism (CD45.2 cells) in peripheral blood of CD45.1 recipient mice ($n = 10$ animal recipients). **c**, Immunofluorescent staining and confocal imaging of injured hearts of CD45.1 recipient animals demonstrating colocalization of GPNMB with DsRed CD45.2 (arrowheads, representative images) (note absence of DsRed fluorescence in nontransplanted but injured animals). Scale bars, 10 µm. **d**, Fraction of DsRed$^+$ GPNMB cells as a fraction of total number of GPNMB cells in infarcted hearts of nontransplanted CD45.1 mice or CD45.1 animals that received CD45.2-DsRed marrow ($n = 2$ CD45.1 mice and $n = 3$ CD45.1 transplanted mice, two-tailed Student's t-test, $^*P < 0.0001$). **e**, Flow cytometry of nonmyocytes isolated from the injured heart at 7 days following injury demonstrating GPNMB is expressed predominantly in DsRed CD45.2$^+$ cells (94.3% versus 0.02%, $n = 3$ animals per group). All data are represented as mean ± s.e.m.

GPNMB plays a critical role in regulating cardiac repair

To determine the role of GPNMB in cardiac repair, we adopted a genetic loss-of-function approach. We generated a mouse deficient in GPNMB (C57BL/6 background) where the GPNMB gene had been knocked out (KO) by homologous recombination approaches. Animals deficient in GPNMB for both alleles (GPNMB KO animal) were born at an expected frequency and did not harbor any cardiac or other obvious abnormalities. The cardiac contractile and electrical activity of the GPNMB KO animals was normal and ECG tracings as well as intervals were not significantly different compared to wild-type (WT) littermates (Extended Data Fig. 3a,b). We subjected 8–12-week-old GPNMB KO animals and age-matched WT littermates to MI and observed that the GPNMB KO animals exhibited a significantly higher mortality (WT 7% versus GPNMB KO 30%, $P < 0.028$) within 7–10 days of LAD ligation mainly due to cardiac rupture (Fig. 3a,b). To decrease high mortality and study the biology of cardiac repair in GPNMB KO animals in greater detail, we induced smaller infarcts by ligating the LAD more distally in both the GPNMB KO and WT littermates. Serial echocardiography was performed at 1, 2 and 4 weeks and we observed that the GPNMB KO animals exhibited significant reduction in cardiac contractile function compared to WT littermates. Ejection fraction (EF) and fractional shortening (FS) were significantly reduced by 7 days of injury with deficits persisting at

4 weeks after injury (Fig. 3c,d). Analysis of EF at 4 weeks demonstrated that 28.6% of the animals in the GPNMB KO had severe depression of EF (EF < 20%) compared to only 7.1% of animals in WT littermates (Fig. 3e). Histology of hearts, collected at 4 weeks after injury and stained with Masson's trichome to determine the area of scarring, demonstrated a significantly greater degree of fibrosis in the GPNMB KO animals (Fig. 3f,g). We characterized the degree of fibrosis as mild (<20%), moderate (20–40%) or severe (>40% of LV surface area) and observed that approximately 67% of GPNMB KO animals exhibited severe fibrosis compared to 8% in WT littermates (Fig. 3h). Post-infarct hypertrophy is associated with an adverse prognosis and measurement of surface area of myocytes in the infarct border zone demonstrated significantly greater size of peri-infarct myocytes in the GPNMB KO animals versus WT control littermates (Fig. 3i,j). Taken together, these observations demonstrate that GPNMB plays a critical role in post-infarct cardiac repair and loss of GPNMB increases mortality and results in significant worsening of post-infarct heart function and fibrosis.

We next investigated the physiological basis of cardiac rupture and worsening contractile function in GPNMB KO animals. As increased myocyte death could underlie both cardiac rupture and worsening contractile function, we performed triphenyltetrazolium chloride (TTC) staining on WT and GPNMB KO hearts on day 3 after moderate MI and observed an almost twofold increase of myocyte death in infarcted hearts of GPNMB KO mice compared to WT animals (Extended Data Fig. 4a,b). Determination of area of risk also by Evans blue staining did not demonstrate any significant differences between WT and GPNMB KO animals suggesting that differences in vascularity in the heart likely did not underlie such differences (Extended Data Fig. 4c,d). As GPNMB was predominantly expressed by myeloid cells, we also examined whether the loss of GPNMB altered bone-marrow myeloid numbers. First, we examined blood counts and did not see any differences in complete and differential blood counts between GPNMB KO and WT animals (Supplementary Table 1). We performed flow cytometry for important macrophage subset markers such as CD206, CD11b, CD68 and Ly6A/E in bone-marrow macrophages derived from GPNMB KO and WT littermates but did not observe any significant difference in bone-marrow macrophage composition between WT and GPNMB KO animals (Extended Data Fig. 5a), demonstrating that GPNMB is less likely to have any impact on myeloid composition in the bone marrow. Flow cytometry for immune cells in peripheral blood demonstrated marginally higher T cell counts in GPNMB KO consistent with previous published reports of effects of GPNMB on T cell proliferation[20] with no significant changes to other immune populations (Extended Data Fig. 5b). We also examined macrophage composition in the uninfarcted hearts of GPNMB KO and WT animals but did not observe significant differences between them (Extended Data Fig. 6).

Single-nuclear transcriptomics of the heart demonstrates a pleiotropic role of GPNMB in post-infarct heart repair

We next performed single-nuclear transcriptomics to determine how GPNMB affects the transcriptional response to cardiac repair in different populations of cells in the infarcted heart. For this purpose, we subjected GPNMB KO and WT littermates to MI and then collected hearts at 7 days following cardiac injury. Nuclei were collected from the hearts and subjected to single-nuclear RNA sequencing (snRNA-seq) using the 10x genomics platform. Cell populations in the infarcted heart were identified by expression of canonical markers of cell identity (Extended Data Fig. 7) and we observed different populations of cell including cardiomyocytes, fibroblasts, inflammatory cells and other nonmyocytes (Fig. 4a). Distribution of WT and GPNMB KO genotypes across these population clusters did not reveal any significant differences in cell numbers in any specific cell population between the two genotypes (Fig. 4b,c). We first confirmed the lack of GPNMB expression in the GPNMB KO animals (Fig. 4d) and that GPNMB was expressed by inflammatory cells and principally by macrophages (Fig. 4e,f). As the source of GPNMB in the infarcted heart was from bone-marrow-derived myeloid cells, we next subclustered the myeloid cells of injured hearts using our scRNA transcriptomic data and analyzed the clusters that abundantly expressed GPNMB (Extended Data Fig. 8a–c). We observed that the majority of GPNMB-expressing myeloid cells in the injured myocardium expressed the singular marker FABP5, which was not expressed (or was minimally expressed) in non-GPNMB-expressing populations (Extended Data Fig. 8d). FABP5 has been shown to be associated with suppression of proinflammatory macrophage activity and these observations suggest that subsets of monocytes regulating or suppressing inflammation in the infarcted heart express GPNMB. We also examined macrophage subsets in humans[21] and observed that GPNMB was expressed in human macrophages enriched in TREM2, which are known to be immunoregulatory[22] (Extended Data Fig. 8e,f). We next examined transcriptional differences in myocytes and pathway analysis demonstrated that GPNMB KO animals exhibited downregulation of pathways associated with cardiac muscle contraction, adrenergic signaling and cardiomyocyte hypertrophy, suggesting that GPNMB promotes the maintenance of expression of cardiac contractile genes in the post-infarct heart (Fig. 4g). Genes known to promote cardiac contraction and adrenergic signaling such as cardiac myosin heavy chain genes, cardiac actinin and troponin were significantly downregulated in infarcted GPNMB KO hearts compared to infarcted WT hearts (Fig. 4h). The downregulation of contractile signaling pathways in myocytes of GPNMB KO animals following infarction is consistent with the phenotype of high mortality, cardiac rupture and rapid development of post-MI cardiac dysfunction. We looked at the fibroblast population and similarly observed greater degree expression of extracellular matrix genes in infarcted hearts of GPNMB KO animals compared to controls (Fig. 4i,j). Expression of collagens and myofibroblast activation markers such as Postn was upregulated in fibroblasts in GPNMB KO hearts consistent with the histological phenotype of increased scarring observed in the GPNMB-deficient animals. Collectively, these observations demonstrate that GPNMB plays a critical role in cardiac repair by maintaining expression of cardiac contractile genes in cardiomyocytes and repressing extracellular matrix gene expression in fibroblasts.

GPNMB gain-of-function approach demonstrates superior post-infarct heart function

We next adopted a gain-of-function approach to determine whether increased GPNMB would be associated with enhanced cardiac repair

Fig. 3 | Genetic deletion of GPNMB (GPNMB KO) results in significant worsening of post-infarct cardiac function. a, Kaplan–Meier curve demonstrating survival of GPNMB KO or WT littermates within the first 30 days after MI ($n = 30$, $^*P < 0.028$, log-rank Mantel–Cox test). **b**, Gross picture of heart of WT animal and GPNMB KO animal at day 7 after MI. Representative GPNMB KO heart showing cardiac rupture (red arrowhead) with a thread passed through the epicardial surface of the rupture seen to traverse to the myocardial chamber confirming transmural rupture in the GPNMB KO animals. **c**, B-mode and M-mode echocardiogram demonstrating poor contractile function with increased chamber dilatation in GPNMB KO animals at 4 weeks following cardiac injury (orange arrows, diastole; blue arrows, systole). **d**, EF and FS over 4 weeks after cardiac injury in WT and GPNMB KO animals ($n = 12$ animals per group; two-way ANOVA with Tukey's multiple comparison; $^*P < 0.035$, $^{**}P < 0.01$). **e**, Pie chart demonstrating the fraction of animals with mild, moderate and severe reductions in EF. **f**, Masson's trichrome staining demonstrating the scar area (blue, arrowheads) in the apical region of the heart. **g**, Quantitation of fibrotic scar area in the apex of heart ($^*P < 0.0004$, two-tailed Student's t-test, $n = 10$ animals per group). **h**, Pie chart showing the % of animals with mild, moderate and severe fibrosis in apex region of the heart. **i**, Cardiac troponin (red) and wheatgerm agglutinin (green) immunostaining to determine myocyte surface area (arrowheads) adjacent to the scar. Scale bars, 50 µm. **j**, Quantitation of myocyte surface area ($^*P < 0.0043$, two-tailed Student's t-test, $n = 6$ animals per group). All data are represented as mean ± s.e.m.

https://doi.org/10.1038/s44161-024-00555-4

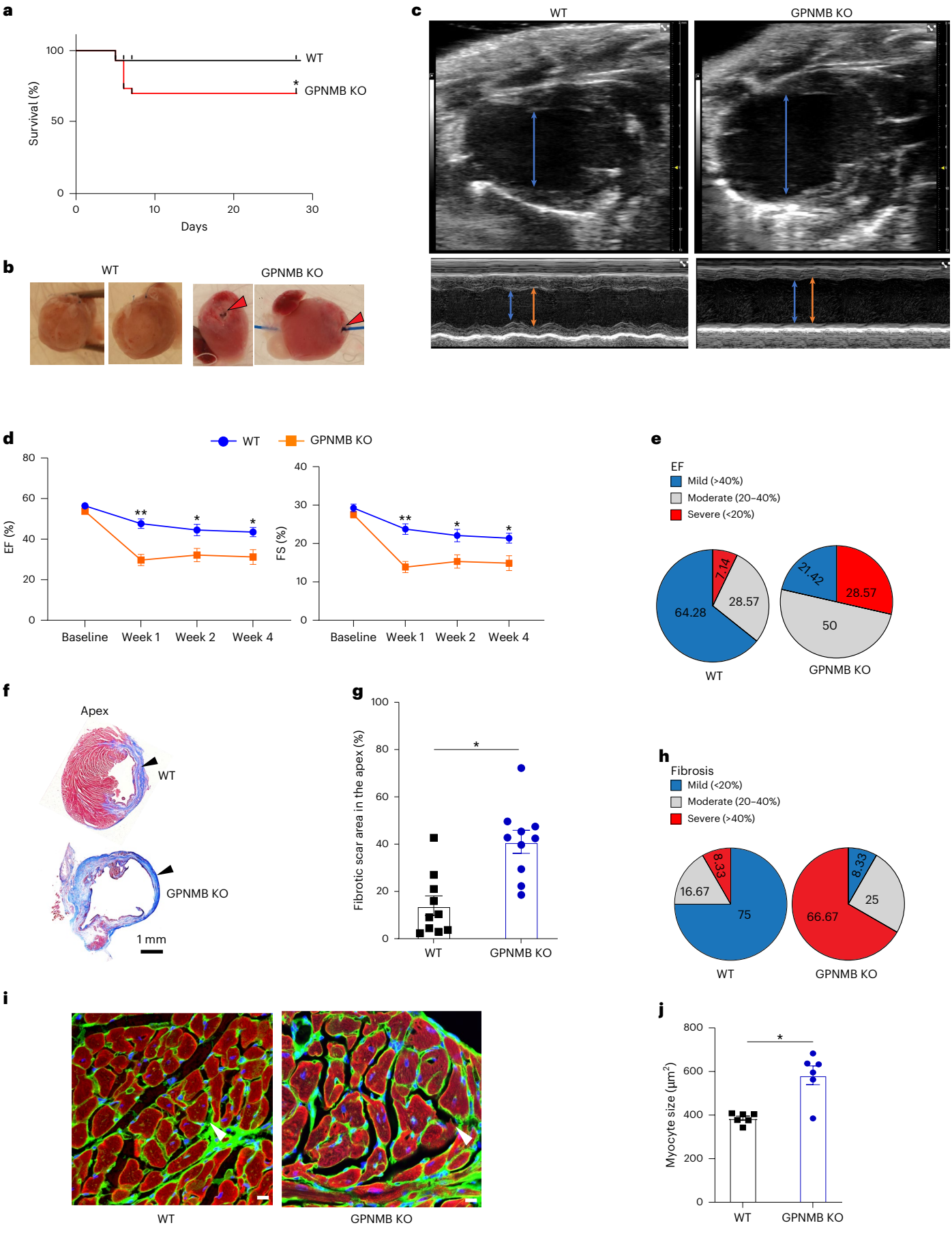

https://doi.org/10.1038/s44161-024-00555-4

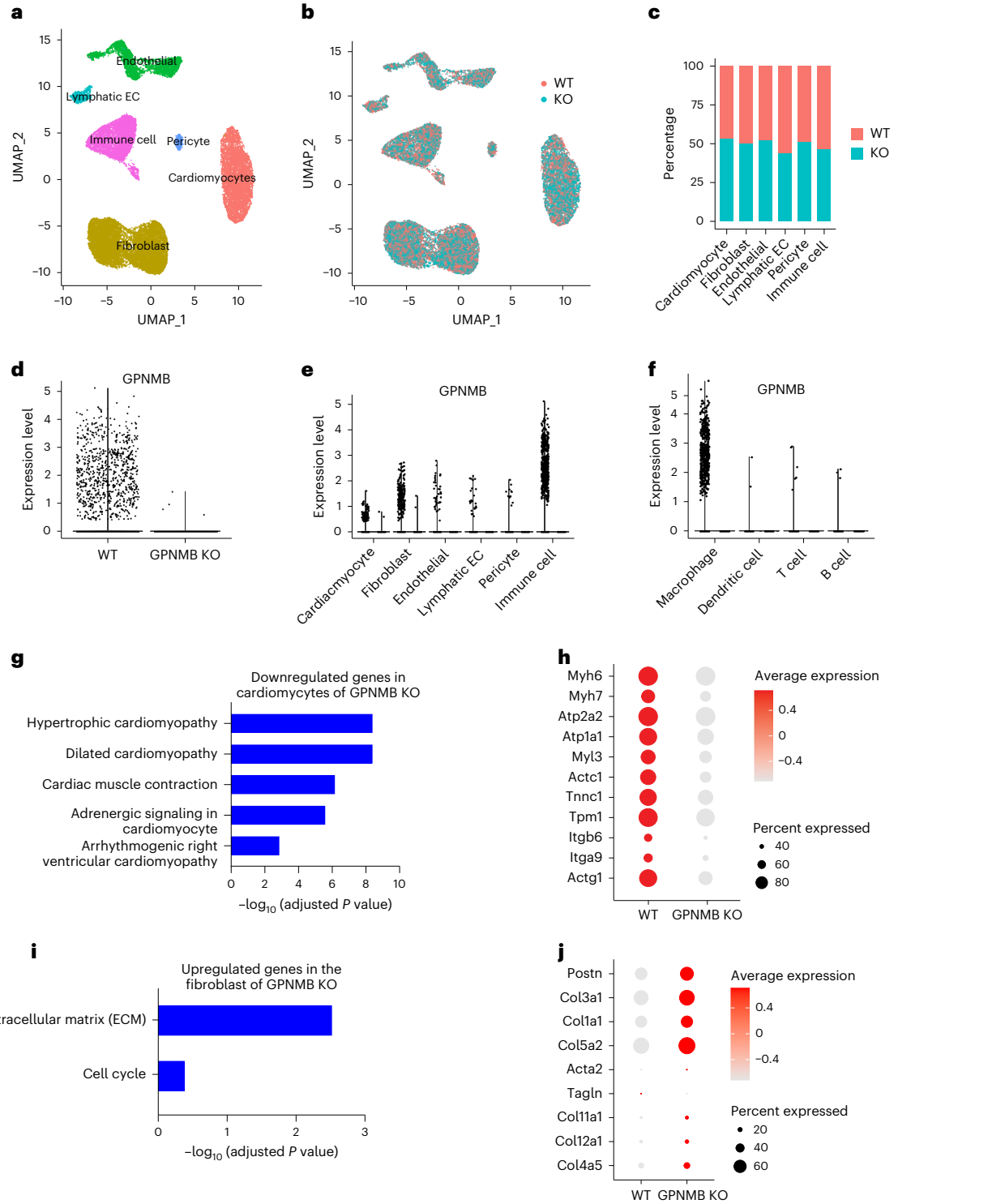

Fig. 4 | Single-nuclear RNA-seq of myocyte and nonmyocyte cells in WT and GPNMB KO animals 7 days after cardiac injury. a, UMAP of different cell-type clusters in the injured heart. EC, endothelial cells. **b**, Distribution of cell clusters between WT and GPNMB KO genotypes. **c**, Percentage of different cell types between WT and KO hearts at 7 days following injury. **d**–**f**, Violin plot demonstrating overall (**d**), cell-type-specific (**e**) and inflammatory-cell-specific (**f**) expressions of GPNMB in WT and GPNMB KO animals. **g**, Enrichr GO analysis of differentially expressed genes (DEGs) in cardiomyocytes of WT and GPNMB KO animals in KEGG domain. **h**, Dot plot of downregulated genes between WT and KO cardiomyocytes. **i**, Enrichr GO analysis of DEGs in cardiac fibroblast of WT and GPNMB KO animals in the KEGG domain. **j**, Dot plot of upregulated genes in the fibroblast of WT and GPNMB KO animals. $n = 4$ animals per group. DEGs were defined by adjusted $P < 0.05$.

and superior post-infarct heart function. GPNMB-ECD mediates biological effects. The ADAM group of proteases is thought to cleave GPNMB with the ECD released into the extracellular space and thus GPNMB-ECD behaves as a secreted factor that can exert biological effects on different cell types. Using adeno-associated virus (AAV8), we overexpressed GPNMB-ECD in the liver. Two weeks after delivery, we confirmed increased GPNMB-ECD expression in the liver by western blotting (Fig. 5a) as well as in the circulation 6 weeks later (Fig. 5b).

https://doi.org/10.1038/s44161-024-00555-4

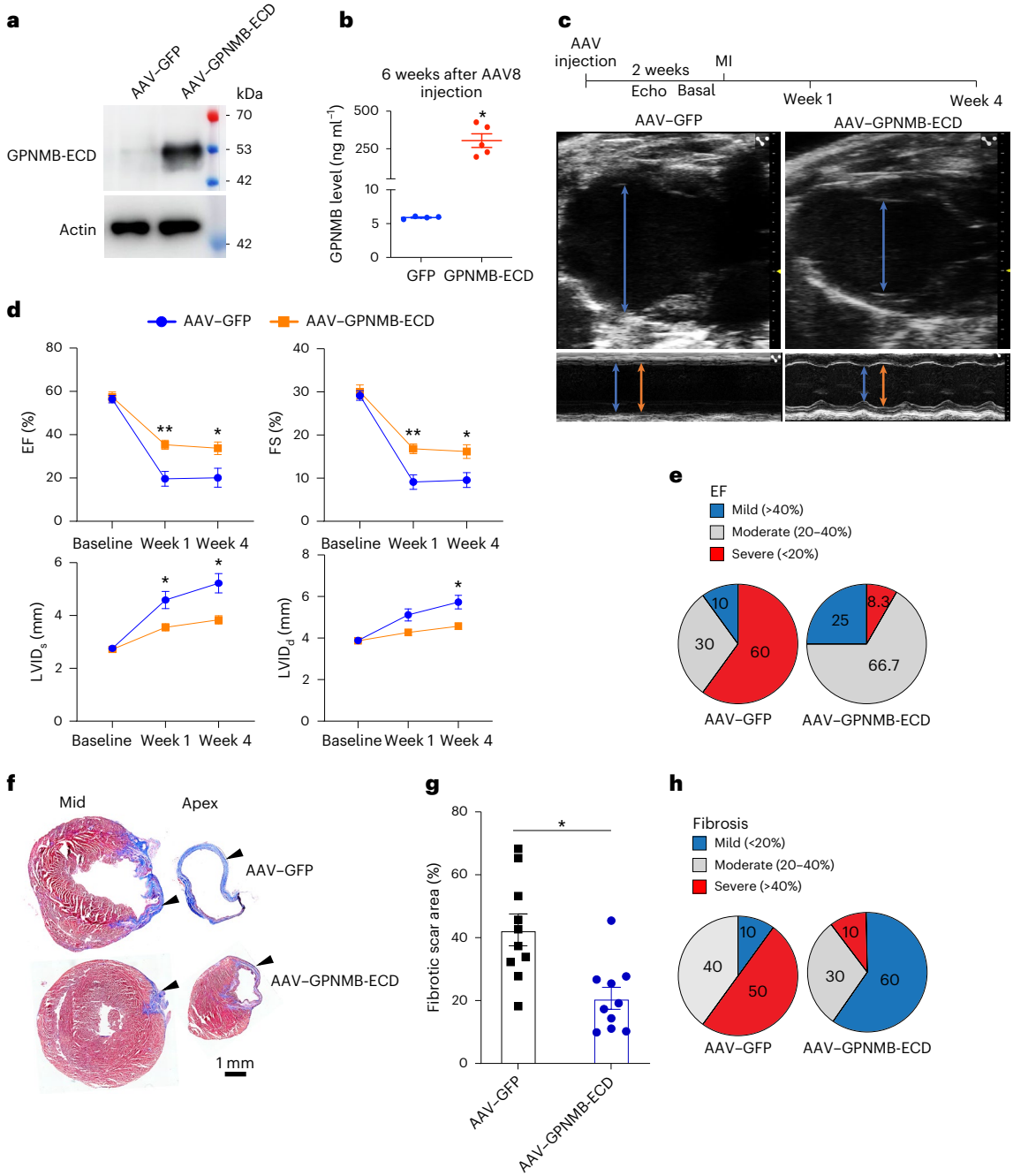

Fig. 5 | Liver-specific overexpression of GPNMB-ECD significantly augments post-infarct cardiac function. a, Western blot demonstrating GPNMB-ECD expression in the liver 2 weeks following intravenous delivery of AAV8–GFP and AAV8–GPNMB-ECD (2×10^{12} GC per animal), $n = 2$. **b**, Circulating levels of GPNMB-ECD in the mice injected with AAV8–GFP and AAV8–GPNMB-ECD at 6 weeks after injection (mean ± s.e.m.; two-tailed Student's *t*-test; $^{*}P < 0.05$, $n = 4$ AAV8–GFP and 5 AAV8–GPNMB-ECD). **c**, B-mode and M-mode echocardiogram indicating superior contractile function with diminished chamber dilatation at 4 weeks following cardiac injury in AAV–GPNMB-ECD animals (orange arrows, diastole; blue arrows, systole). **d**, EF and FS and LV chamber size (LVID) in systole (LVID$_s$) and diastole (LVID$_d$) over 4 weeks after cardiac injury in AAV8–GFP and AAV8–GPNMB-ECD animals (baseline $n = 14$ per group, GFP week 1 $n = 12$, week 4 $n = 10$, GPNMB-ECD week 1 $n = 12$, week 4 $n = 12$; two-way ANOVA with Tukey's multiple comparison; $^{*}P < 0.05$, $^{**}P < 0.016$). **e**, Pie chart demonstrating the fraction of animals with mild, moderate and severe reductions in EF (AAV8–GFP $n = 10$ and AAV8–GPNMB $n = 12$). **f**, Masson's trichrome staining demonstrating the scar (blue, arrowheads) in the apex and mid-ventricle. **g**, Quantitation of fibrotic scar area in the apex and mid-ventricle ($n = 10$ animals per group, two-tailed Student's *t*-test, $^{*}P < 0.0365$). **h**, Pie chart showing the % of animals with mild, moderate and severe fibrosis. All data are represented as mean ± s.e.m.

We next subjected the animals that received AAV8–GPNMB-ECD or control AAV8–GFP to MI, 2 weeks after viral delivery. Echocardiography demonstrated significantly superior post-infarct contractile function in the animals that received AAV8–GPNMB-ECD compared to animals that received control AAV8–GFP virus (Fig. 5c,d). Animals that received GPNMB-ECD exhibited significantly superior EF and FS at 1 week after MI with cardiac functional benefits persisting through 4 weeks (Fig. 5c,d). Animals that received GPNMB-ECD also exhibited decreased ventricular dilatation following infarction (Fig. 5d). We examined the number of animals that exhibited severe depression of post-infarct EF and observed that the number of animals that exhibited severe post-infarct heart failure was significantly decreased in

https://doi.org/10.1038/s44161-024-00555-4

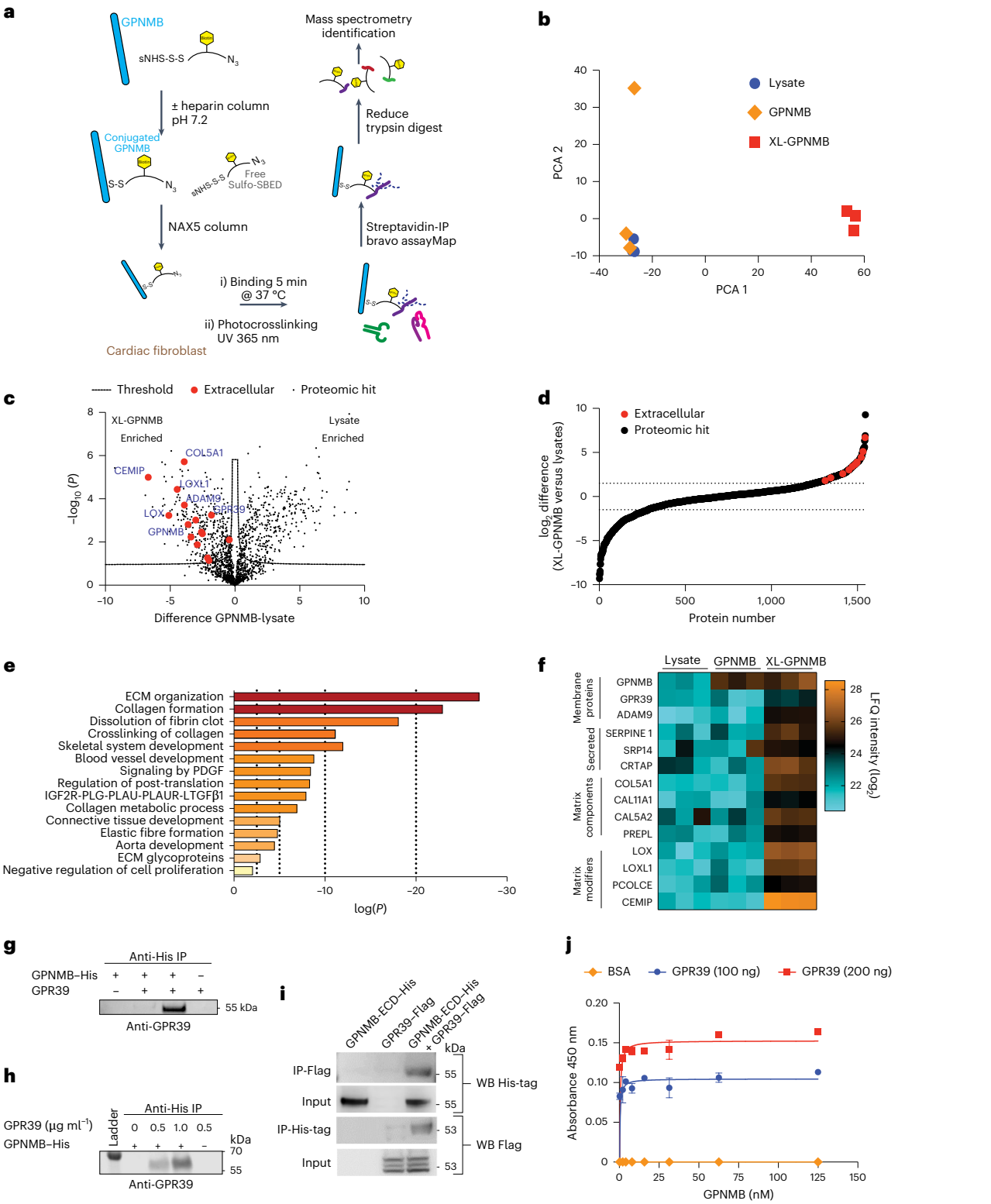

Fig. 6 | GPNMB-ECD interacts with the G-coupled receptor, GPR39. **a**, Sulfo-SBED biotin proteomic workflow. **b**, Principal-component analysis (PCA) of the proteomic hits of the cell lysate, uncrosslinked Sulfo-SBED biotin GPNMB and crosslinked (XL) Sulfo-SBED biotin GPNMB (XL-GPNMB) pulldown. **c**, Volcano plot of protein peptide enriched in the crosslinked (XL)-GPNMB streptavidin-IP compared to peptide hit in proteomic analysis of total cell lysate input from murine cardiac fibroblasts performed ($n = 3$). Statistically significant changes between groups were assessed by two-way ANOVA with a permutation-based false discovery rate for multiple test correction. **d**, The number of protein peptides and their relative enrichment to total lysates in the mass spectrometry analysis. **e**, Metascape analysis of the protein peptides enriched 1.5-fold in the XL-GPNMB compared to total lysate. ECM, extracellular matrix. **f**, Heat map of label-free quantification (LFQ) intensities of selected candidate protein peptides identified in the proteomic screens. **g**,**h**, Immunoprecipitation (IP) of His-tagged GPNMB in the presence or absence of recombinant GPR39 in liposomes. **i**, Western blot (WB) of Co-IP samples indicating the interaction between GPNMB-ECD and GPR39 in the cell lysates of HEK293 cells coexpressing GPNMB-ECD and GPR39. **j**, μg ml^{-1} ELISA binding assay of BSA and GPNMB to coupled GPR39 at the indicated concentrations. All data are shown as mean ± s.e.m. ($n = 2$).

https://doi.org/10.1038/s44161-024-00555-4

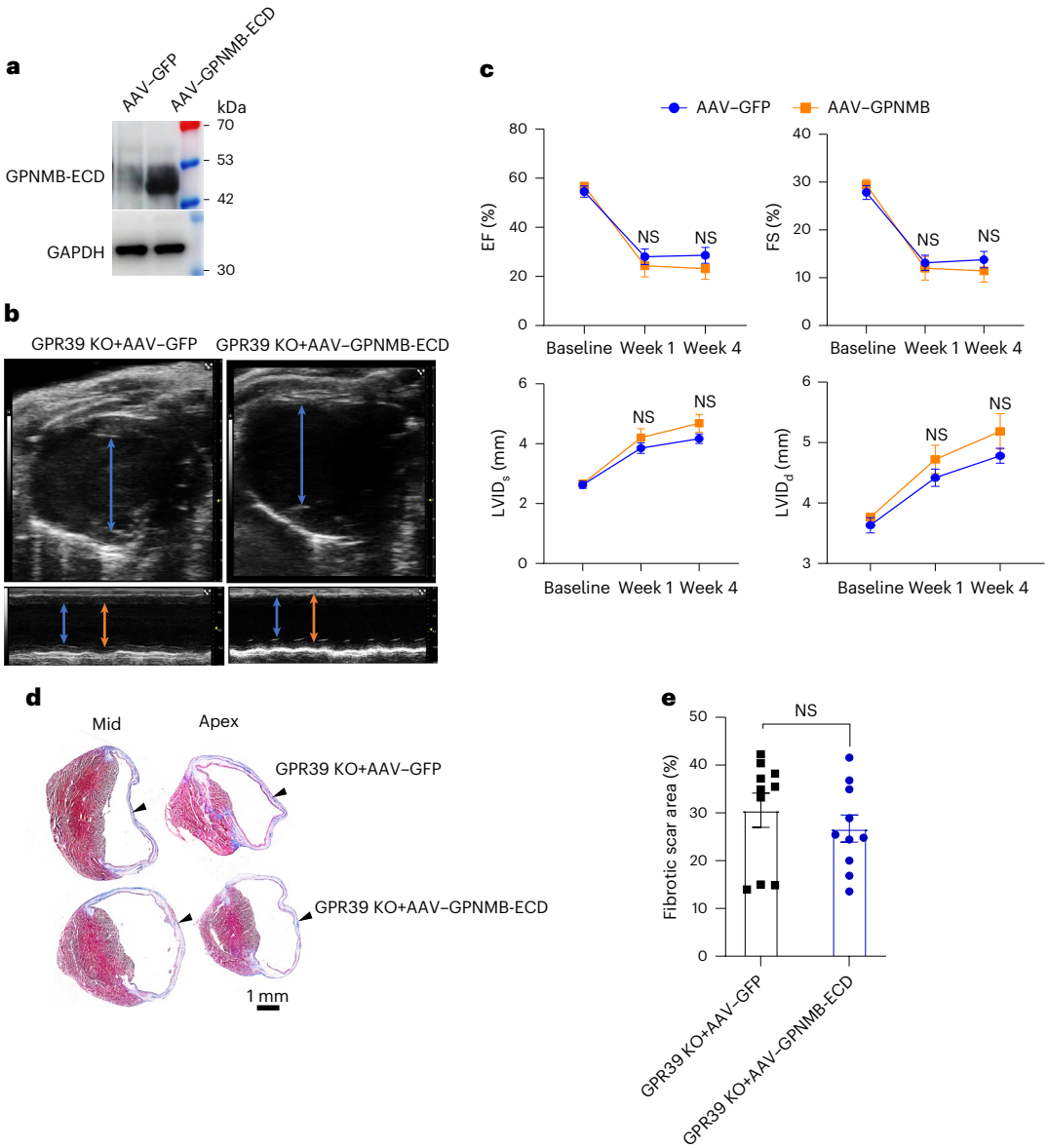

Fig. 7 | GPNMB-ECD failed to elicit a cardioprotective function in GPR39 KO animals. a, Western blot demonstrating GPNMB-ECD expression in the liver 2 weeks following intravenous delivery of AAV8–GFP and AAV8–GPNMB-ECD (2×10^{12} GC per animal), $n = 2$. **b**, B-mode and M-mode echocardiogram demonstrating poor contractile function with chamber dilatation at 4 weeks of cardiac injury in GPR39 KO mice that received AAV8–GFP and AAV8–GPNMB-ECD (orange arrows, diastole; blue arrows, systole). **c**, EF and FS and LV chamber size (LVID) in systole and diastole over 4 weeks after cardiac injury in GPR39 KO + AAV–GFP and GPR39 KO + AAV–GPNMB-ECD animals (GFP baseline $n = 11$, week 1 $n = 11$, week 4 $n = 11$; GPNMB-ECD baseline $n = 14$, week 1 $n = 12$, week 4 $n = 12$; two-way ANOVA with Tukey's multiple comparison). **d**, Masson's trichrome staining demonstrating the scar (blue, arrowheads) in the apex and mid-ventricle. **e**, Quantitation of fibrotic scar area in the apex and mid-ventricle ($n = 10$; two-tailed Student's t-test; NS, not significant). All data are represented as mean ± s.e.m.

animals that received AAV8–GPNMB-ECD (8.3% versus 60%) (Fig. 5e). We collected the hearts at 4 weeks following MI and Masson's trichrome staining demonstrated significant decrease in scarring in animals that received GPNMB-ECD (Fig. 5f,g). We also examined the severity or degree of cardiac fibrosis at 4 weeks after MI and observed that only 10% of animals in the AAV8–GPNMB-ECD group developed severe fibrosis (>40% of LV surface area) compared to 50% in control AAV8–GFP animals (Fig. 5h). Taken together, these gain-of-function experiments demonstrate the beneficial effects of increased circulating GPNMB-ECD on cardiac repair.

GPR39 serves as a receptor for the GPNMB-ECD ligand

GPNMB-ECD is heavily glycosylated and has an integrin binding domain with which it is thought to bind to integrin receptors; however, the GPNMB-ECD is also proteolytically released and can serve as an extracellular ligand potentially capable of exerting effects on multiple cell types in the infarcted niche. Given our observation that GPNMB-ECD exerts beneficial effects on post-infarct repair and cardiac function, we next sought to identify the receptor that binds to GPNMB-ECD. For this purpose, we performed a proteomic workflow using chemical crosslinking affinity purification and mass spectrometry with the Sulfo-SBED biotin crosslinked to the GPNMB extracellular domain. In brief, a Sulfo-SBED biotin moiety was initially crosslinked to GPNMB-ECD (Fig. 6a). To avoid loss of heparan sulfate or chondroitin sulfate interactions, we conjugated the Sulfo-SBED biotin to GPNMB-ECD bound on a heparin column to protect lysine residues on GPNMB critical for heparan sulfate binding (Fig. 6b). GPNMB-ECD conjugated to the Sulfo-SBED biotin was then added to cardiac primary fibroblasts and crosslinked using UV

https://doi.org/10.1038/s44161-024-00555-4

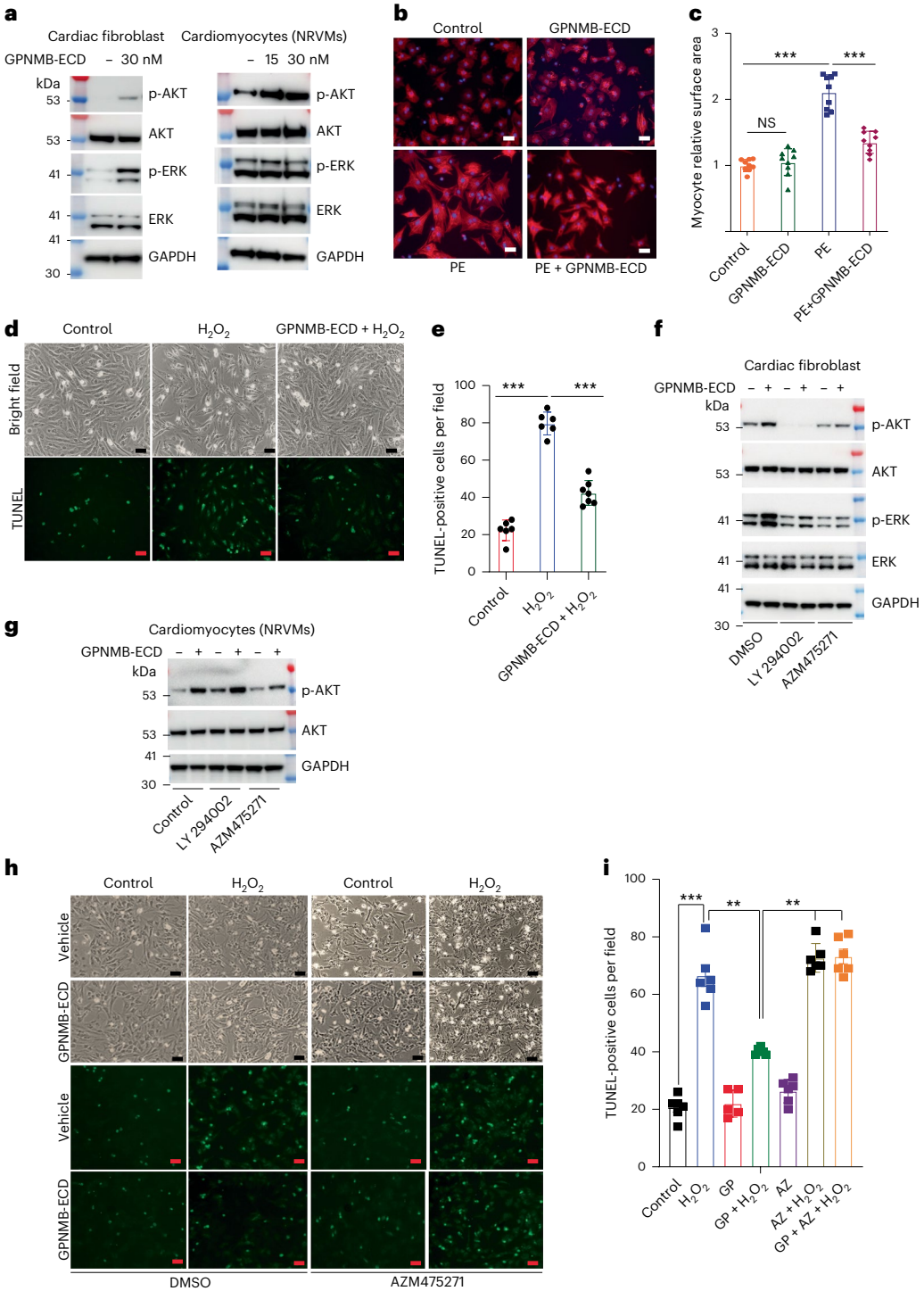

Fig. 8 | GPNMB-ECD activates AKT and ERK signaling of heart cells through PI3 and src kinase-dependent mechanisms and prevents cardiomyocyte hypertrophy and apoptosis. a, Western blot demonstrating phosphorylated and total AKT and ERK, and GAPDH proteins in the cell lysates of control and GPNMB-ECD-treated cardiac fibroblasts and NRVMs. **b**, Immunofluorescence of troponin expression demonstrating cardiomyocytes surface area under control, phenylephrine (PE), GPNMB-ECD and PE + GPNMB-ECD-treated conditions. Scale bars, 10 µm. **c**, Quantitative measurement of relative myocyte surface area under various treatment conditions as indicated (mean ± s.e.m.; $n = 9$ independent samples; $^{***}P < 0.0001$ by one-way ANOVA with Tukey's multiple comparison; NS, not significant). **d**, Bright-field and immunofluorescence images indicating cardiomyocyte death under control, H_2O_2 and GPNMB-ECD + H_2O_2-exposed conditions. Scale bars, 10 µm. **e**, Quantifications of TUNEL-positive cells under various treatment conditions (mean ± s.e.m.; $n = 6$ independent samples; $^{***}P < 0.0001$ by one-way ANOVA with Tukey's multiple comparison). **f**, Western blot demonstrating the expression of phosphorylated and total AKT and ERK proteins and GAPDH in the cell lysates of cardiac fibroblasts under various treatments as indicated in the blot. DMSO, dimethylsulfoxide. **g**, Immunoblotting of phosphorylated and total AKT proteins and GAPDH in the cell lysates of NRVMs exposed to GPNMB-ECD with or without PI3 and src kinase inhibitors as indicated in the blot. **h**, Bright-field and immunofluorescence images indicating cardiomyocyte death under various treatment conditions as determined by TUNEL assay. Scale bars, 10 µm. **i**, Quantifications of TUNEL-positive cells (mean ± s.e.m.; $n = 6$; $^{**}P < 0.0003$, $^{***}P < 0.0001$ by one-way ANOVA with Tukey's multiple comparison). Drugs and concentrations were GPNMB-ECD (GP) 30 nM, PE 10 µM, H_2O_2 100 µM, LY294002 10 µM and AZM475521 (AZ) 1 µM.

exposure after 5 min. This would thus generate a complex where the Sulfo-SBED moiety would link the GPNMB-ECD and potentially interacting proteins. Cells were subsequently lysed and the GPNMB-ECD pulled out with a streptavidin biotin system and subjected to mass spectrometry to identify proteins that interact with GPNMB. GPNMB not crosslinked to Sulfo-SBED moiety served as controls. Proteomic analysis of the lysate, GPNMB-ECD pulldown with (XL-GPNMB) and without crosslinking (GPNMB) revealed identification of a different pool of interacting proteins (Fig. 6b). Of the 1,546 murine proteins identified, we observed 282 proteins to be uniquely enriched >1.5-fold after GPNMB crosslinking (Fig. 6c–f). Extracellular proteins associated with extracellular matrix deposition, assembly and matrix modifications were significantly enriched in the lysate pulldown following GPNMB crosslinking (Fig. 6c,d). Gene Ontology (GO) analysis identified most of the proteins to be associated with extracellular matrix, collagens and glycoproteins (Fig. 6e). We then functionally classified the top hits and of the extracellular proteins identified, including the protease ADAM9, we identified GPR39 as the only cell-surface signaling receptor (Fig. 6f). GPR39 is a G-coupled receptor known to be modulated by zinc[23,24]. No endogenous protein ligands have been identified to bind GPR39. To confirm this interaction, we subsequently performed immunoprecipitation experiments using His-tagged GPNMB-ECD in the presence and absence of liposomes with GPR39. Nickle column pulldown of GPNMB-ECD revealed a specific and dose dependent GPNMB–GPR39 interaction (Fig. 6g,h). To further confirm the results obtained by proteomic workflow and cell-free binding assays, we examined whether GPNMB-ECD interacted with GPR39 in mammalian cells that coexpress them. We overexpressed both GPNMB-ECD–His-tag and GPR39–Flag in HEK293 cells by transient transfection. The cell lysates were immunoprecipitated with anti-Flag or anti-His-tag antibodies and probed for GPNMB–His-tag or GPR39–Flag, respectively. These immunoprecipitation experiments revealed that anti-Flag antibody coprecipitates GPNMB–His-tag protein and anti-His-tag antibody pulled down GPR39–Flag protein as shown in the western blots (Fig. 6i) confirming the physical interaction between GPNMB-ECD and GPR39. In addition, to determine binding affinity of GPNMB-ECD to GPR39, we performed a modified binding ELISA assay and coated plates with two concentrations of GPR39 to evaluate binding of soluble His-tagged GPNMB-ECD. The results showed a dose dependent binding of GPNMB to GPR39 with a K_d of approximately 3.8 nM (Fig. 6j). In conclusion, using different but synergistic methodological approaches, we identified the GPNMB-ECD as an endogenous ligand for GPR39.

Animals deficient in GPR39 do not exhibit beneficial post-MI effects of injected AAV8–GPNMB-ECD

Having identified GPR39 as a potential receptor for GPNMB-ECD ligand, we next determined the physiological role of GPR39 in mediating the beneficial effects of GPNMB after infarction. For this purpose, we injected AAV8–GPNMB-ECD or AAV8–GFP into animals that are deficient in GPR39 (GPR39 KO animals, C57BL/6 background). GPR39 KO animals do not display any obvious cardiac abnormalities following homozygous deletion of GPR39 and did not demonstrate any abnormalities of cardiac function at baseline (Extended Data Fig. 9)[25]. Two weeks following AAV8–GFP or AAV8–GPNMB-ECD injection, we confirmed the expression of GPNMB-ECD in the liver (Fig. 7a) and subjected the animals to MI. Echocardiography did not demonstrate any differences in cardiac contractile function or LV chamber size between GPR39 KO mice that received AAV8–GFP or AAV8–GPNMB-ECD (Fig. 7b,c). This is in contrast to WT mice (same genetic background) that demonstrated a significant benefit following injection of AAV8–GPNMB-ECD (Fig. 5d). Hearts were collected at 4 weeks and Masson's trichrome staining did not demonstrate any significant differences in the degree of fibrosis in GPR39 KO animals that received GPNMB-ECD versus GFP (Fig. 7d,e). These findings suggest that increased levels of GPNMB mediate their beneficial effects on cardiac repair via GPR39. We next subjected the GPR39 KO and WT littermates to MI but did not observe any significant differences in cardiac function (Extended Data Fig. 10). Taken together these observations suggest that while GPR39 mediates the beneficial effects of GPNMB-ECD, transmembrane-bound GPNMB expressed on macrophages can potentially bind to other receptors to mediate the beneficial physiological effects, or functional redundancy exists between the receptors that bind to GPNMB.

GPNMB-ECD activates AKT and ERK phosphorylation in cardiac cells and attenuates myocyte hypertrophy and apoptosis

Our genetic loss- and gain-of-function experiments demonstrate that GPNMB exerts beneficial effects on the infarcted heart. The snRNA transcriptomic profiling demonstrated differential expression of genes in myocytes and fibroblasts of GPNMB KO animals suggesting that GPNMB predominantly affects myocytes and fibroblasts in the infarcted heart. To gain insight into the molecular signaling mechanisms downstream of GPNMB, we performed in vitro experiments to determine the effects of GPNMB on cardiac fibroblasts and myocytes. Earlier reports suggested that GPNMB-ECD can activate AKT and ERK phosphorylation in NSC-34 cells, neuroblastoma and spinal cord hybrid cells in vitro[26]. AKT phosphorylation has been considered to be cardioprotective with anti-apoptotic and anti-fibrotic effects[27–29]. We checked the expression of p-AKT and p-ERK in GPNMB- ECD-exposed cardiac fibroblast and neonatal rat ventricular myocytes (NRVMs) by western blotting. We observed that GPNMB-ECD activated both AKT and ERK phosphorylation in cardiac fibroblasts and induced AKT phosphorylation in cardiomyocytes (Fig. 8a), indicating a cell-autonomous response to GPNMB. Next to determine the functional significance of the GPNMB–AKT axis in pathological myocyte hypertrophy and death, we treated NRVMs with phenylephrine, which is known to induce cardiac hypertrophy in the presence or absence of GPNMB-ECD. Consistent with the protective effects of GPNMB in vivo, GPNMB-ECD protected cardiomyocytes from phenylephrine-induced hypertrophy (Fig. 8b,c). As MI is associated with myocyte death, we also treated cardiomyocytes with H_2O_2, which induces rapid cell death of myocytes. We observed that GPNMB-ECD protected cardiomyocytes from H_2O_2-induced apoptosis (Fig. 8d,e). It is known that cell-surface signaling events can activate AKT and ERK phosphorylation through various kinases, including PI3 and src. To specifically identify the downstream kinase that mediates GPNMB-induced AKT and ERK phosphorylation, we treated cardiac fibroblasts and myocytes with GPNMB-ECD in the presence of PI3 and src kinase inhibitors LY294002 and AZM475271, respectively. While both inhibitors prevented the GPNMB-ECD-induced ERK and AKT phosphorylation in cardiac fibroblasts, only the src kinase inhibitor abrogated the AKT phosphorylation induced by GPNMB-ECD in NRVMs (Fig. 8f,g). These observations demonstrate cell-autonomous or cell-specific responses of downstream signaling kinases to GPNMB stimulation of the heart. Consistent with the GPNMB signaling mechanisms identified by us, the src inhibitor AZM475271 abrogated the protective effects of GPNMB-ECD on H_2O_2-induced myocyte apoptosis (Fig. 8h,i). Taken together, these experiments suggest that downstream stimulation of the AKT–ERK pathways mediated by the PI3 and src kinases mediates in part the phenotypic effects of GPNMB on cardiomyocytes and fibroblasts.

Discussion

Our observations support the critical role of macrophage-derived GPNMB in regulating cardiac repair after MI. GPNMB is known to be expressed by diverse population of cells in different tissues, but our experiments suggest that bone-marrow-derived macrophages are the primary source of GPNMB in the infarcted heart. Genetic loss-of-function experiments demonstrated that animals deficient in GPNMB exhibited rapid development of heart failure after MI and exhibited much higher mortality than control animals. This was in part due to a greater degree of myocyte cell death and cardiac rupture.

Cardiac cell populations in the hearts of GPNMB-deficient animals exhibited transcriptional changes in both myocyte and nonmyocyte populations of cells suggestive of pleiotropic effects of GPNMB on different cell populations in the infarcted region. Although GPNMB was originally identified in cancer cell lines, the roles of GPNMB in regulating cell growth, inflammation and tissue repair have been recently uncovered[30]. The pro-repair effects of GPNMB observed in our study are broadly consistent with the effects of GPNMB in accelerating repair of bones after fractures[12]. Our observations not only show a necessity for GPNMB for optimal cardiac repair but also a pharmacological use of GPNMB in enhancing cardiac repair, as increasing circulating GPNMB-ECD was sufficient to enhance cardiac repair and lead to superior post-infarct heart function.

It is to be noted that GPNMB is a single-pass transmembrane protein and its integrin binding domain residing within the extracellular domain is thought to bind to integrin and other glycoproteins such as CD44 to mediate cellular events[31]; however, the extracellular domain is also cleaved by the ADAM group of proteases and when released from the cell surface can exert its effects. The effects of membrane-bound GPNMB versus the free GPNMB-ECD are not well understood but the observations made in this study would suggest that increasing GPNMB-ECD circulating levels is sufficient to exert beneficial effects on cardiac repair. A distinct role of the membrane-bound GPNMB cannot be ruled out in our study, but it is possible that the circulating form of GPNMB-ECD alone mediates the beneficial results of GPNMB on the infarcted heart. In this regard, crosslinking and immunoprecipitation studies identified the orphan receptor GPR39 as a receptor that bound to the GPNMB-ECD with high affinity. Genetic deletion of GPR39 abrogated the beneficial cardiac effects of over-expressing GPNMB-ECD, thereby suggesting that GPNMB-ECD mediated its beneficial effects on the infarcted heart via GPR39; however, GPR39 KO mice did not demonstrate any worsening of cardiac function when compared to WT littermates. These observations would suggest that there is functional redundancy in the types of receptors that GPNMB-ECD can bind, or that the membrane form of GPNMB binds to different receptors than the GPNMB-ECD.

Methods

Animal studies

All animal studies were approved by the Animal Research Committee (ARC) of the University of California, Los Angeles (UCLA) and all animals were maintained at the UCLA vivarium in accordance with the policies laid out by the Association for Assessment and Accreditation of Laboratory Animal Care.

Genetically engineered GPNMB KO and GPR39 KO animals and murine models of cardiac injury. Mice that were globally deficient of GPNMB (C57BL/6 background) were generated from GPNMB KO embryos obtained from KOMP repository. The entire coding region of the *GPNMB* gene was replaced by neo cassette by a traditional homologous recombination approach. GPR39 KO mice generated on a C57BL/6 background were obtained from B. Holst, University of Copenhagen. MI was performed by permanent ligation of the LAD coronary artery after open thoracotomy as described earlier[17]. All the supplies and instruments used for the surgery were sterile. In brief, animals were anesthetized with ketamine (80 mg kg^{-1}, intraperitoneally (i.p.)) and xylazine (20 mg kg^{-1}, i.p.) and respiration was provided through mechanical ventilation with 95% O_2 (tidal volume 0.5 ml, 130 breaths per min). The LAD coronary artery was ligated intramurally 2 mm or below from its origin with a 9-0 proline suture. The position of the suture determines the severity of injury and a more distal tie of the artery was employed to decrease the severity of infarction. Sham animals underwent the same procedure except for ligation of the vessels. Intubation was achieved orally and a small incision in the anterior neck was made to reveal the trachea to facilitate cannulation of the upper airway. At the end, the chest was closed and animals were observed during recovery from anesthesia. Mice were kept on a heating plate until full recovery from anesthesia.

Total RNA isolation and qPCR. Scar and remote tissue collected at different time points after MI were used to extract RNA using an RNeasy Mini kit (QIAGEN, 74104) followed by complementary DNA synthesis by iScript (Bio-Rad, 170-8891). The cDNA was used to quantify the expression of GPNMB and GAPDH with specific primers. Real-time PCR was run on 96-well plates using a SYBR Premix ExTaq II (TAKARA) according to the instructions of the manufacturer. Relative gene expression levels were quantified using the Thermal Cycler Dice Real-Time System II software (TAKARA). The following gene-specific primer pairs were used for qPCR; mGPNMB-F CTACAACTGGACTGCAGGGG, mGPNMB-R TTTCTTCCATCCATGGGGGC, mGAPDH-F TGCACCACCAACTGCTTAGC and mGAPDH-R GGCATGGACTGTGGTCATGA.

Western blotting. Approximately 20 mg heart tissue was lysed in 500 µl RIPA buffer (Thermo Fisher Scientific, 89901) containing protease and phosphatase inhibitors (Thermo Fisher Scientific, 78443) in a tissue lyser. Cell pellets of NRVMs and cardiac fibroblasts collected after various treatments were lysed with NP-40 lysis buffer containing protease and phosphatase inhibitors. The lysates were centrifuged at 15,000*g* for 15 min at 4 °C and the supernatants were collected for a BCA assay (Thermo Fisher Scientific, 23225). Equal amounts of total protein (10–30 µg) for each sample were separated on 4–12% Bis-Tris gels (Invitrogen, NP0323) using an electroblotting apparatus (Thermo Fisher Scientific, NW2000) and transferred onto to a PVDF membrane (GE Healthcare, 45-004-095). The membrane was blocked in 5% milk for 60 min and incubated with primary antibodies at 4 °C overnight. Protein signals were detected using HRP-conjugated secondary antibodies (Cell Signaling Technologies) and SuperSignal West Femto western blotting detection reagents (Thermo Fisher Scientific, 34094).

Antibodies. The primary antibodies used for immunofluorescence staining were: rabbit anti-GPNMB (1:200 dilution, Cell Signaling, 90205); rat anti-CD45 (1:100 dilution, Millipore, 051416); rabbit anti-CD68 (1:100 dilution, Abcam, ab125212); rat anti-CD11b (1:100 dilution, Abcam, ab8878); rat anti-F4/80 (1:100 dilution, Invitrogen, MA191124); rat anti-CD31 (1:200 dilution, Abcam, ab7388); rabbit anti-CD146 (1:200 dilution, Abcam, ab75769); rabbit anti-NG2 (1:200 dilution, Millipore, AB5320); rat anti-CD90.2 (1:50 dilution, BD Biosciences, 566082); rabbit anti-cardiac troponin I (1:100 dilution, Abcam, ab47003); and Alexa Fluor 594 conjugated wheatgerm agglutinin (5 µg ml^{-1}, Invitrogen, W11262).

For flow cytometry, APC-conjugated anti-CD45 (1:100 dilution, BioLegend, 103111); APC-conjugated anti-CD68 (1:100 dilution, BioLegend, 137007); APC-conjugated anti-CD11b (1:100 dilution, Invitrogen, 13011281); Alexa Fluor anti-GPNMB (1:100 dilution, Abcam, Ab284639); Brilliant Violet anti-CD11b (1:100 dilution, BioLegend, 101235); PE anti-CD3 (1;100 dilution, BioLegend, 100205); FITC anti-CD19 (1:100 dilution, BioLegend 101505); FITC-anti-Ly-6A/E (1:100 dilution, Thermo Fisher Scientific, 11-5981-82); Alexa Flour anti-CD206 (1:100 dilution, Thermo Fisher Scientific, 53-2061-82); APC-conjugated anti-Ly-6C (1:100 dilution, BioLegend, 128015); and eFluor anti-GPNMB (1:100 dilution, Invitrogen, 50-5708-82).

For western blotting, the following primary antibodies were used: rabbit anti-p-AKT (Ser 473) (1:2,000 dilution, Cell Signaling, 4060), rabbit anti-p-ERK (1:1,500 dilution, Cell Signaling, 4695), rabbit anti-AKT (1:2,000 dilution, Cell Signaling, 4691), mouse anti-ERK (1:1,000 dilution, Sata Cruz, 514302), goat anti-GPNMB (1:1,000 dilution, R&D Systems, AF2330), rabbit anti-GAPDH (1:2,000 dilution, Cell Signaling, 2118), mouse anti-Flag (1:1,000 dilution, Proteintech, 66008-3Ig) and rabbit anti-His-tag (1:1,000 dilution, Proteintech, 10001-0-AP).

Single-cell RNA sequencing. Single-cell RNA sequencing data of nonmyocytes at day 7 after MI in C57BL/6 WT mice presented in this paper (Fig. 1g,i) were analyzed from a previously published dataset[18] (scRNA-seq data GSE152122).

Histological analysis of the heart and confocal microscopy. To collect the heart for histological studies, the LV was perfused with 5 ml PBS followed by 2 ml of 4% paraformaldehyde (PFA). Then the hearts were post-fixed in 4% PFA for additional 4 h, subsequently subjected to dehydration in sucrose solution, snap frozen in Tissue-Tek O.C.T compound (SAKURA, 4583) and sectioned at 10 µm-thickness.

For immunofluorescence staining, frozen tissue sections were incubated with pre-chilled acetone at −20 °C for 10 min, blocked in 10% species-specific normal serum in 1% BSA/PBS for 1 h and stained with primary antibodies at 4 °C overnight. After washing three times with PBS, the sections were incubated with fluorescent-conjugated secondary antibodies for 1 h followed by washing an additional three times with PBS. Finally, sections were mounted with SlowFade Gold Antifade reagent (Invitrogen, S36936) including 4,6-diamidino-2-phenylindole (DAPI; 1 µg ml^{-1}, Invitrogen, D3571) to counterstain nuclei and imaged with a confocal microscope (Eclipse Ti2, Nikon).

For Masson's trichrome staining, sections were stained using a Masson's trichrome stain kit (Thermo Fisher Scientific, 22-110-648). Images were taken of heart sections from the apex and mid-ventricle and the fibrotic area was quantified using ImageJ. The scar tissue area was calculated as the fraction of the LV surface area occupied by the scar tissue. The severity of fibrosis was classified as 'severe' (sample showed >40% fibrotic area), 'moderate' (20–40%) or 'mild' (<20%). The cross-sectional cardiomyocyte size was calculated using cells with integral membrane and visible nucleus (≈60 cells per section). Relative fibrotic area and cardiomyocyte size quantification was performed using ImageJ (v.1.49) software.

Flow cytometry. Nonmyocyte cells were isolated from the injured region of the heart on day 7 after MI in the same manner as described before[17]. Isolated nonmyocytes were resuspended 100–300 µl 1% BSA in PBS and incubated with various fluorescent-conjugated antibodies specific for each cell types and subtypes for about 30 min 4 °C. After washing with FACS buffer twice, stained cells were analyzed on an LSRII IMED (BD Biosciences) or sorted on a FACS Aria II (BD Biosciences).

For lineage-tracing experiments, an equal number of male and female B6.129(Cg)-*Cx3cr1*^{tm1Litt}*Ccr2*$^{tm2.1Ifc}$/JernJ (Ccr2^{RFP}Cx3cr1^{GFP}) mice procured from The Jackson Laboratory were infarcted, and on day 7 nonmyocyte cells were isolated from the injured region of the heart for flow cytometry analysis as described above.

To identify the resident macrophage composition in the uninjured heart, nonmyocyte cells were isolated from the WT and GPNMB KO animals and subjected to flow cytometry using the fluorescent-conjugated antibodies specific for resident macrophage populations.

Bone-marrow macrophages purified from age- and sex-matched WT and GPNMB KO mice were cultured for 7 days in macrophage growth medium (DMEM with 10% FBS, 10 ng ml^{-1} M-CSF and antibiotics). Then the cells were collected by trypsinization and incubated with various fluorescence conjugated antibodies to identify the percentage of various macrophage compositions by flow cytometry. The peripheral immune cell composition between WT and GPNMB KO animals were determined by flow cytometry using the blood drawn through retro-orbital puncture. All the flow cytometry data were analyzed using FlowJo v.10.4 software.

Bone-marrow transplantation and engraftment analysis. SJL CD45.1 male mice at approximately 10–11 weeks old were irradiated at 900 cGy with a cesium irradiator. The next day, bone marrow was collected from femurs and tibias of two 9-week-old DsRed CD45.2 male donors (JAX Strain 006051 B6.Cg-Tg(CAG-DsRed*MST)1Nagy/J). Then, a single-cell suspension was prepared using IMDM supplemented with 10% FBS + 10% penicillin/streptomycin. The suspension was centrifuged at 200*g* for 5 min and supernatant was aspirated. Red blood cells were lysed in 2 ml ACK lysis buffer for 10 min. Cell suspension was filtered through a 30-µm filter and neutralized with complete medium to a total volume of 10 ml. Cells were counted and kept on ice. Each recipient SJL CD45.1 mouse received 3 × 10^6 DsRed CD45.2 donor cells intravenously in 200 µl through tail vein injections. For the engraftment analysis, 100 µl peripheral blood was collected in Eppendorf tubes with PBS + 10% FBS and 4 µl EDTA to prevent clotting. Red blood cells were lysed in 2 ml ACK lysis buffer for 10 min. Suspension was centrifuged at 200*g* for 5 min and supernatant was aspirated. Cells were stained with each antibody in FACS buffer (1% BSA in PBS) with one drop of UtraComp eBeads Compensation Beads (Thermo Fisher Scientific, 01-2222-42) for 30 min at 4 °C. Then, 5 µl 7-AAD was added before running the samples. After washing with FACS buffer twice, stained cells were analyzed on Canto II FACS instrument (BD Biosciences) with BD FACS DIVA software. Data were analyzed using FlowJo v.10.4 software.

Echocardiographic analysis. Echocardiographic imaging was performed under 1.5% isoflurane anesthesia on a heated platform using a Vevo 3100 Imaging System with a 30-MHz linear probe (Visualsonics), short–long axis B-mode and M-mode images were captured and analyzed by Vevo 3100 software. Heart rates were also recorded.

Isolation of nuclei, library construction and sequencing. Hearts collected from WT and GPNMB KO mice on day 7 after myocardial injury were used for the nuclei isolation/purification and 10x genomics sequencing. In brief, freshly collected heart tissue was minced on ice in a sterile Petri dish with a razor blade and homogenized with chilled lysis buffer (10 mM Tris-HCl (pH 7.4), 10 mM NaCl, 3 mM $MgCl_2$ and 0.1% NP-40) using a Dounce homogenizer. The tissue homogenate was then passed through a 40-µm cell strainer and centrifuged at 500*g* for 5 min at 4 °C. The supernatant was carefully removed and the pellet was resuspended with 1 ml nuclei wash buffer (1× PBS with 2% BSA and 0.2 U ml^{-1} RNase inhibitor). The suspension was filtered through a 20-µm pluristrainer and centrifuged at 500*g* for 5 min at 4 °C. The nuclei pellet was resuspended in 300 µl nuclei wash buffer (PBS with 2% BSA and 0.2 U ml^{-1} RNase inhibitor) and submitted for library preparation and sequencing. After determining the quality and quantity of the purified nuclei, equal number of nuclei from each sample were used to construct single nuclei gene expression libraries using Chromium Next GEM (Gel Beads-in-emulsion) Single-Cell 3′ (v3.1 Chemistry) (10x Genomics), Chromium Next GEM Chip G Single-Cell kit (10x Genomics) and Single Index Kit T Set A (10x Genomics) according to the manufacturer's instructions. In brief, purified nuclei samples were loaded to target at least 10,000 nuclei to form GEMs and barcode nucleus of individual cells. Then the GEMs were cleaned and cDNA libraries were created as per the manufacturer's guidelines. The quality of the constructed library was determined using 4200 Tape Station System (Agilent) and D1000 ScreenTape (Agilent) and Qubit 4 2.0 (Invitrogen) for concentration and size distribution. After confirming the quality, samples were sequenced using Novaseq 6000 (Illumina) using 100 cycles and 200 M reads for each sample, targeting about 20,000 reads per nuclei. Finally, the samples were analyzed using Cell Ranger and Loupe (10x Genomics). For the analysis of sequencing data, the R package Seurat (v.3.1.2) was used to cluster the nucleus (cells) in the merged matrix. Low-quality nuclei were eliminated if they had subnormal (fewer than 100 genes) or more than 2 × 10^4 transcripts or 2% of mitochondrial genes. To normalize the expression levels, The NormalizeData function was used for each cell with default parameters. The FindVariableFeatures function was used to select variable genes with default parameters. The ScaleData function was used to scale and center the counts in the dataset and principal-component analysis was

performed on the variable genes. The batch effect was removed using The RunHarmony function from the Harmony package. The RunUMAP function was used for Uniform Manifold Approximation and Projection (UMAP) dimensional reduction. The clusters were obtained using the FindNeighbors and FindClusters functions with the resolution set to 0.6. The cell cluster markers were found using the FindAllMarkers function. The dot plot and violin plots were plotted using the DotPlot and VlnPlot functions, respectively. Enrichr was used for pathway enrichment analysis on the differentially expressed genes[32].

Adeno-associated virus 8 production and injection. AAV8 encoding GFP or GPNMB-ECD was purchased from VectorBuilder. The animals were injected with AAV8–GFP and AAV8–GPNMB-ECD (2×10^{12} genome copies (GC) in 100 µl per animal) intravenously via the tail vein following a standard procedure[33,34]. Two weeks after the virus injection, the liver tissue was collected from randomly selected animals and a western blot was performed to check GPNMB-ECD overexpression. Once overexpression was confirmed, the animals were subjected to myocardial injury. The circulating levels of GPNMB-ECD were also checked 6 weeks after AAV injection to confirm the stable expression of GPNMB-ECD throughout the study period.

Peripheral blood ELISA for GPNMB. We assessed circulating GPNMB levels 6 weeks after AAV8 injection. Plasma samples were collected by retro-orbital puncture at the time of killing in plastic blood-collection tubes with sodium heparin (BD 367874). Plasma GPNMB levels were measured using commercially available ELISAs kit as described by the manufacturer (R&D systems, DY2330).

Sulfo-SBED crosslinking proteomics. GPNMB labeled with Sulfo-SBED biotin (Pierce) was prepared by first loading GPNMB onto a heparin Sepharose column to block the GPNMB heparan sulfate binding site from being labeled by the NHS linker. The column was then loaded with 1.7 mM Sulfo-SBED biotin and the reaction was allowed to proceed at 4 °C for 2 h. The column was then thoroughly washed with low-salt buffer (25 mM HEPES and 100 mM NaCl, pH 7.5) to remove the unreacted linker and then labeled protein was eluted with high-salt buffer (25 mM HEPES and 800 mM NaCl, pH 7.5). Labeled GPNMB was then buffer exchanged into PBS using a PD-10 desalting column. Primary cardiac fibroblasts were cultured in F12k culture medium with 20% FBS and 10 ng ml^{-1} h-bFG. Cells were then serum starved for 24 h, washed three times with F12k culture medium and incubated with 100 nM of Sulfo-SBED biotin GPNMB conjugates for 5 min at 37 °C. Then, cells were washed with serum-free medium and placed on ice. Cells were crosslinked for 15 min using a UV Stratalinker 1800 (Stratagene). Cells were then washed twice more with PBS, lysed and collected with RIPA buffer.

Sample preparation. Proteins were quantified by BCA assay (Thermo Fisher Scientific) as per manufacturer recommendations. A total of 3 mg of protein extract from each sample was used for affinity purification of biotinylated proteins. Affinity purification was carried out in a Bravo AssayMap platform (Agilent) using AssayMap streptavidin cartridges (Agilent). In brief, cartridges were first primed with 50 mM ammonium bicarbonate and then proteins were slowly loaded onto the streptavidin cartridge. Background contamination was removed by extensively washing the cartridges with 8 M urea and 50 mM ammonium bicarbonate. Finally, cartridges were washed with Rapid digestion buffer (Promega, Rapid digestion buffer kit) and proteins were subjected to on-cartridge digestion with mass spectrometry-grade trypsin/Lys-C Rapid digestion enzyme (Promega) at 70 °C for 2 h. Digested peptides were then desalted in the Bravo platform using AssayMap C18 cartridges and the organic solvent was removed in a SpeedVac concentrator before liquid chromatography–tandem mass spectrometry (LC–MS/MS) analysis.

LC–MS/MS analysis. Dried peptides were reconstituted with 2% acetonitrile and 0.1% formic acid, quantified by modified BCA peptide assay (Thermo Fisher Scientific) and analyzed by LC–MS/MS using a Proxeon EASY nanoLC system (Thermo Fisher Scientific) coupled to a Q-Exactive Plus mass spectrometer (Thermo Fisher Scientific). Peptides were separated using an analytical C18 Acclaim PepMap column 0.075 × 500 mm, 2-µm particles (Thermo Fisher Scientific) in a 93-min linear gradient of 2–28% solvent B at a flow rate of 300 nl min^{-1}. The mass spectrometer was operated in positive data-dependent acquisition mode. MS1 spectra were measured with a resolution of 70,000, an AGC target of 1×10^6 and a mass range from 350 to 1,700 m/z. Up to 12 MS2 spectra per duty cycle were triggered, fragmented by HCD and acquired with a resolution of 17,500 and an AGC target of 5×10^4, an isolation window of 1.6 m/z and a normalized collision energy of 25. Dynamic exclusion was enabled with duration of 20 s. Data were processed using MaxQuant (v.1.6.3.4). Data were searched against the mouse genome with peptide and protein false discovery rate set to 0.01. Full search parameters are included in the Supplementary Information (mqpar.xml file). Peptide-level data are provided in allPeptides.txt and protein level information is provided in proteinGroups.txt.

Liposomal immunoprecipitation. Recombinant GPNMB was incubated in the presence or absence of recombinant GRP39 liposomes (Abnova, H00002863-G01) in buffer (150 mM NaCl, 5 mM $CaCl_2$, 5 mM $MgCl_2$ and 20 mM HEPES, pH 7.5) for 30 min at room temperature. GPNMB–GPR39 complexes were then pulled down using magnetic hydrophilic streptavidin beads (NEB) conjugated with His-tag biotinylated antibody (R&D Systems, cat. no. BAM050, lot DXN1422112). Beads were washed 3× with buffer and protein was then eluted with citric acid and NuPage LDS buffer (Invitrogen). Western blot was used to detect the presence of GPR39 (Novus rabbit anti-GPR39, 1;1,000 dilution, cat. no. NLS139, lot A-6).

ELISA. ELISA plates were coated with 100 or 200 ng GPR39 in liposomes (Abnova H00002863-G01) in a total volume of 50 µl and incubated overnight at 4 °C. After coating, the wells were emptied and washed once with 150 µl of wash buffer (150 mM NaCl, 5 mM $MgCl_2$, 5 mM $CaCl_2$ and 20 mM HEPES at pH 7.2) per well. Subsequently, 150 µl of blocking buffer was added to each well and the plates were incubated for 1 h at room temperature with gentle shaking to block nonspecific binding sites. For the detection assay, a threefold dilution series of GPNMB ranging from 100 nM to 1.58 nM was prepared in binding/blocking buffer and 50 µl was added to each well. After the incubation, the plates were washed three times with 150 µl of wash buffer per well. Avidin–HRP conjugate was diluted 1:2,000 in binding/blocking buffer and 50 µl was added to each well, followed by three washes using 150 µl per well of TSM washing buffer (20 mM Tris-HCl, 150 mM NaCl, 1 mM $CaCl_2$ and 1 mM $MgCl_2$, pH 7.4). The plates were developed by adding 50 µl of TMB substrate to each well and allowing the reaction to proceed for 15 min. The reaction was stopped by adding 50 µl of 2 M H_2SO_4 to each well. The absorbance was measured at 450 nm using a microplate reader.

Plasmid construction and verification. Full-length cDNA clone for mouse GPNMB (BC026375) was purchased from GE Dharmacon. The cDNA fragment encoding the N-terminal extracellular domain (amino acids 1–502) was amplified and tagged with 6xHis at the C terminus by PCR and cloned into XbaI-BamHI enzymatic sites of pHIV–EGFP (Addgene, #21373). Primers for PCR were: GCGGCCGCTGAGTTAACTATTCTAGAACCATGGAAAGTCTCTGCGGGGTC and GGGGAGGGAGAGGGGCGGATCCTTAgtgatggtgatggtgatgATTCACTGCTCTCAGAGG. The correct assembly of the plasmid was confirmed through Sanger sequencing. A lentiviral vector with puromycin resistance marker, pHIV–EGFP–P2A–PuroR, was created by inserting a P2A-PuroR fragment (amplified from Addgene, #98290 with PCR primers CTGTACAAGGGATCCGGCGCAACAAAC and ATGTATCGATCGTGCGCTCCTTTCGGT)

into the EGFP C terminus of a pHIV–EGFP vector (Addgene, #21373, between BsrGI and ClaI sites) by restriction cloning. A plasmid harboring mouse GPR39 cDNA (NM_027677.2) with a C-terminal Flag tag was purchased from VectorBuilder. The GPR39–Flag fragment was amplified by PCR (primers: ATTCTAGAGCCACCATGGCTTCATCCAGTG and AGCCCGGGTCACTTGTCGTCATCGTCT) and cloned between the XbaI and XmaI sites of the above pHIV–EGFP–P2A–PuroR vector. Correct assembly and the GPR39–Flag sequence were confirmed by Sanger sequencing.

Co-immunoprecipitation. HEK293 cells were cultured in DMEM (Gibco, 11995065) containing 10% FBS and antibiotics (100 U ml^{-1} penicillin + 100 µg ml^{-1} streptomycin). HEK293 cells grown in a 10-cm dish were transfected with 1 µg of either pHIV–EGFP–GPNMB-ECD–His or pHIV–EGFP–GPR39–Flag plasmid individually or together using FuGENE HD transfection reagent (Promega, E2311). Two days after transfection, cells were used for co-immunoprecipitation (Co-IP) experiments using a Capturem IP- and Co-IP kit (Takara, 635721) according to the manufacturer's instructions. Mouse anti-Flag (Proteintech, 66008-3Ig) and rabbit anti-His-tag (Proteintech, 10001-0-AP) antibodies were used for the pulldown and subsequent western blot analysis.

Expression and purification of recombinant mGPNMB-ECD. HEK293 cell grown in 10-cm plates were transfected with 1.5 µg of pHIV–EGFP–GPNMB-ECD plasmid using FuGENE HD transfection reagent (Promega, E2311) as per the manufacturer instructions. Three days after transfection, the culture medium and cell pellets were collected and used for the purification of His-tag–mGPNMB-ECD utilizing the Capturem His-tagged Purification Maxiprep kit (Takara, 635713) following the manufacturer's instruction. The purity of mGPNMB-ECD was verified by western blot.

Neonatal rat ventricular cardiomyocyte isolation and culture. NRVMs were isolated as previously described[35] in accordance with UCLA IACUC guidelines. In brief, 0–2-day-old rat (Sprague–Dawley) pups were killed by decapitation, rinsed briefly in ethanol and the hearts were excised. The hearts were washed in Hanks–HEPES solution to remove the blood then the ventricles were isolated by removing the atria using small scissors. Isolated ventricles were transferred to another dish and minced into small pieces using sterile razor blade. The minced tissues were digested with a collagenase–pancreatin solution for 30 min at 37 °C in a shaking incubator. Myocytes were enriched and purified by discontinuous Percoll gradient centrifugation. The purified NRVMs were then seeded in gelatin (0.2%)-coated culture plates at 1,000 cells per cm^2 in DMEM + 10% FBS + 100 U ml^{-1} penicillin + 100 µg ml^{-1} streptomycin for various treatment and assays.

Isolation of adult cardiac fibroblasts and immortalization. WT mice were killed using an isoflurane inhalation chamber and the hearts were immediately dissected out, rinsed in ice-cold HBSS and the valves and atriums were removed using fine scissors in a sterile biosafety cabinet. The ventricles were minced into small pieces using a sterile razor blade and digested in 0.1 µg ml^{-1} liberase TH (Sigma, 5401151001) in Tyrode's solution (136 mM NaCl, 5.4 mM KCl, 0.33 mM NaH_2PO_4, 1 mM $MgCl_2$, 10 mM HEPES and 0.18% glucose) by incubating in a temperature-controlled orbital shaker at 37 °C for 30 min at 80 rpm while triturating with a 10-ml pipette every 5 min. The digested heart suspension was filtered through a 40-µM strainer and centrifuged at 200*g* for 5 min. The supernatant was discarded and the pellet was resuspended in F-12K (Gibco, 21127022) medium containing 20% FBS and antibiotics and plated in standard tissue culture dishes. Approximately, 2–4 h after plating, the medium was removed and washed with PBS then fresh F12K medium containing 20% FBS, antibiotics and human basic FGF (10 ng ml^{-1}, Millipore, GF003) was added. These cells were immortalized by infecting them with Lentivirus-Large T antigen virus in the presence of Polybrene (8 µg ml^{-1}) and selected with antibiotics (puromycin 1 µg ml^{-1}) as described previously[17]. Immortalized cardiac fibroblasts were then cultured in DMEM (Gibco, 11995065) containing 10% FBS.

Hypertrophy assay. NRVMs cultured in 24-well plates were serum starved for 24 h and then exposed to phenylephrine (10 µM) and GPNMB-ECD (30 nM) individually or in combination for 48 h. After the incubation, the cells were fixed with 4% paraformaldehyde for 10 min at room temperature. The cells were washed with PBST (in PBS containing 0.05% Tween 20) and blocked with immunofluorescence blocking buffer (Cell Signaling, cat. no. 12411) for 1 h followed by incubation with anti-troponin antibody (1:100 dilution) diluted in 1% BSA and PBS at 4 °C overnight. The next day, cells were washed with PBST for 10 min each three times and then incubated with fluorescent-conjugated secondary antibody (1:200 dilution) for 1 h. Cells were counterstained with DAPI (1 mg ml^{-1}, Invitrogen, D3571) for 10 min and mounted with SlowFade Gold Antifade reagent (Invitrogen, S36936). Images were taken using ECHO Revolve Fluorescence Microscope (model no. RVL-100-M) and cell size was measured using ImageJ (v.1.49) software.

Cell death assay. NRVMs cultured in 24-well plates were serum starved for 24 h and then exposed to GPNMB-ECD (30 nM) in the presence and absence of LY294002 (10 µM) (Tocris, 1130) and AZM475271 (1 µM) (Tocris, 3963) for 12 h and then exposed to hydrogen peroxide (100 µM) for 12 h. The cells were washed with PBS and incubated with TUNEL reaction mixture (Roche, 11684795910) for 1 h at 37 °C and washed three times with PBS. The images were acquired in at least 3–5 random fields in each well using an ECHO Revolve Fluorescence Microscope (model no. RVL-100-M). The TUNEL-positive cells were counted using ImageJ (v.1.49) software.

Determination of infarct size by triphenyltetrazolium chloride staining. Mice hearts collected on day 3 after myocardial injury were sliced transversally at a thickness of 1 mm. The sliced tissues were washed in PBS to remove blood and then immersed in neutral TTC (2% in saline) solution for 30 min at 37 °C. The tissues were photographed and the extent of viable versus dead tissue was quantified using ImageJ (v.1.49) software.

Determination and quantification of area at risk by Evans blue staining. WT and GPNMB KO animals were infarcted by LAD ligation and 24 h later 1% Evans blue dye was perfused into the aorta and coronary arteries to stain the nonischemic area. Hearts were excised and sliced into cross sections and the area of blue staining was quantified by ImageJ (v.1.49) software.

Human dataset analysis. GPNMB was plotted in the human macrophage and monocyte atlas datasets (https://macroverse.gustaveroussy.fr/2021_MoMac_VERSE/) curated by Mulder et al.[21].

Statistics. All experimental results are expressed as mean ± s.e.m. Statistical significance between two experimental groups was determined using either one or two-way analysis of variance (ANOVA) with Tukey's multiple comparison or a Student's two-tailed *t*-test as indicated in figure legends. *P* values < 0.05 were considered statistically significant. Statistical analyses were performed using GraphPad Prism v.7.02 software. All data are presented as mean ± s.e.m.

Reporting summary

Further information on research design is available in the Nature Portfolio Reporting Summary linked to this article.

Data availability

The snRNA-seq data generated for this study were deposited in the Gene Expression Omnibus under accession numbers GSE235434 and GSE277086.

References

1. Frangogiannis, N. G. Pathophysiology of myocardial infarction. *Compr. Physiol.* **5**, 1841–1875 (2015).
2. Frangogiannis, N. G. Emerging roles for macrophages in cardiac injury: cytoprotection, repair, and regeneration. *J. Clin. Invest.* **125**, 2927–2930 (2015).
3. Tzahor, E. & Dimmeler, S. A coalition to heal-the impact of the cardiac microenvironment. *Science* **377**, eabm4443 (2022).
4. Gnecchi, M., Zhang, Z., Ni, A. & Dzau, V. Paracrine mechanisms in adult stem cell signaling and therapy. *Circ. Res.* **103**, 1204–1219 (2008).
5. Weterman, M. A. et al. nmb, a novel gene, is expressed in low-metastatic human melanoma cell lines and xenografts. *Int. J. Cancer* **60**, 73–81 (1995).
6. Tsou, P. S. & Sawalha, A. H. Glycoprotein nonmetastatic melanoma protein B: a key mediator and an emerging therapeutic target in autoimmune diseases. *FASEB J.* **34**, 8810–8823 (2020).
7. Furochi, H. et al. Osteoactivin fragments produced by ectodomain shedding induce MMP-3 expression via ERK pathway in mouse NIH-3T3 fibroblasts. *FEBS Lett.* **581**, 5743–5750 (2007).
8. Lazaratos, A. M., Annis, M. G. & Siegel, P. M. GPNMB: a potent inducer of immunosuppression in cancer. *Oncogene* **41**, 4573–4590 (2022).
9. Zhou, L. et al. Glycoprotein non-metastatic melanoma protein b (Gpnmb) is highly expressed in macrophages of acute injured kidney and promotes M2 macrophages polarization. *Cell Immunol.* **316**, 53–60 (2017).
10. Kumagai, K. et al. Glycoprotein nonmetastatic melanoma B (Gpnmb)-positive macrophages contribute to the balance between fibrosis and fibrolysis during the repair of acute liver injury in mice. *PLoS ONE* **10**, e0143413 (2015).
11. Yu, B., Alboslemy, T., Safadi, F. & Kim, M. H. Glycoprotein nonmelanoma Clone B regulates the crosstalk between macrophages and mesenchymal stem cells toward wound repair. *J. Invest. Dermatol.* **138**, 219–227 (2018).
12. Frara, N. et al. Transgenic expression of Osteoactivin/gpnmb enhances bone formation in vivo and osteoprogenitor differentiation ex vivo. *J. Cell. Physiol.* **231**, 72–83 (2016).
13. Jarve, A. et al. Adverse left ventricular remodeling by glycoprotein nonmetastatic melanoma protein B in myocardial infarction. *FASEB J.* **31**, 556–568 (2017).
14. Lin, L. Y. et al. Systems genetics approach to biomarker discovery: GPNMB and heart failure in mice and humans. *G3* **8**, 3499–3506 (2018).
15. Cordero, P. et al. Pathologic gene network rewiring implicates PPP1R3A as a central regulator in pressure overload heart failure. *Nat. Commun.* **10**, 2760 (2019).
16. Liu, Y. et al. RNA-seq identifies novel myocardial gene expression signatures of heart failure. *Genomics* **105**, 83–89 (2015).
17. Li, S. et al. Cardiomyocytes disrupt pyrimidine biosynthesis in nonmyocytes to regulate heart repair. *J. Clin. Invest.* **132**, e149711 (2022).
18. Yokota, T. et al. Type V collagen in scar tissue regulates the size of scar after heart injury. *Cell* **182**, 545–562.e23 (2020).
19. Dieckmann, B. W., Paguaga, M. E., McCollum, G. W., Penn, J. S. & Uddin, M. I. Role of NLRP3 inflammasomes in monocyte and microglial recruitments in choroidal neovascularization. *ImmunoHorizons* **8**, 363–370 (2024).
20. Chung, J.-S., Sato, K., Dougherty, I. I., Cruz, P. D. Jr. & Ariizumi, K. DC-HIL is a negative regulator of T lymphocyte activation. *Blood* **109**, 4320–4327 (2007).
21. Mulder, K. et al. Cross-tissue single-cell landscape of human monocytes and macrophages in health and disease. *Immunity* **54**, 1883–1900.e1885 (2021).
22. Kim, S. H., Lee, K. Y. & Chang, K. The protective role of TREM2 in the heterogenous population of macrophages during post-myocardial infarction inflammation. *Int. J. Mol. Sci.* **24**, 5556 (2023).
23. Cuzon Carlson, V. C. et al. Modulation of Gpr39, a G-protein coupled receptor associated with alcohol use in non-human primates, curbs ethanol intake in mice. *Neuropsychopharmacology* **44**, 1103–1113 (2019).
24. Dong, X., Tang, S., Zhang, W., Gao, W. & Chen, Y. GPR39 activates proliferation and differentiation of porcine intramuscular preadipocytes through targeting the PI3K/AKT cell signaling pathway. *J. Recept. Signal. Transduct. Res.* **36**, 130–138 (2016).
25. Młyniec, K., Budziszewska, B., Holst, B., Ostachowicz, B. & Nowak, G. GPR39 (zinc receptor) knockout mice exhibit depression-like behavior and CREB/BDNF down-regulation in the hippocampus. *Int. J. Neuropsychopharmacol.* **18**, pyu002 (2014).
26. Ono, Y., Tsuruma, K., Takata, M., Shimazawa, M. & Hara, H. Glycoprotein nonmetastatic melanoma protein B extracellular fragment shows neuroprotective effects and activates the PI3K/Akt and MEK/ERK pathways via the Na^+/K^+-ATPase. *Sci. Rep.* **6**, 23241 (2016).
27. Fujio, Y., Nguyen, T., Wencker, D., Kitsis, R. N. & Walsh, K. Akt promotes survival of cardiomyocytes in vitro and protects against ischemia-reperfusion injury in mouse heart. *Circulation* **101**, 660–667 (2000).
28. Nagoshi, T. et al. PI3K rescues the detrimental effects of chronic Akt activation in the heart during ischemia/reperfusion injury. *J. Clin. Invest.* **115**, 2128–2138 (2005).
29. Qin, W., Cao, L. & Massey, I. Y. Role of PI3K/Akt signaling pathway in cardiac fibrosis. *Mol. Cell. Biochem.* **476**, 4045–4059 (2021).
30. Saade, M., Araujo de Souza, G., Scavone, C. & Kinoshita, P. F. The role of GPNMB in Inflammation. *Front. Immunol.* **12**, 674739 (2021).
31. Taya, M. & Hammes, S. R. Glycoprotein non-metastatic melanoma protein B (GPNMB) and cancer: a novel potential therapeutic target. *Steroids* **133**, 102–107 (2018).
32. Kuleshov, M. V. et al. Enrichr: a comprehensive gene set enrichment analysis web server 2016 update. *Nucleic Acids Res.* **44**, W90–W97 (2016).
33. Wasala, L. P., Hakim, C. H., Yue, Y., Yang, N. N. & Duan, D. Systemic delivery of adeno-associated viral vectors in mice and dogs. *Methods Mol. Biol.* **1937**, 281–294 (2019).
34. Li, S. et al. Metabolic reprogramming and epigenetic changes of vital organs in SARS-CoV-2-induced systemic toxicity. *JCI Insight* **6**, e145027 (2021).
35. Pereira, A. H. M., Cardoso, A. C. & Franchini, K. G. Isolation, culture, and immunostaining of neonatal rat ventricular myocytes. *STAR Protoc.* **2**, 100950 (2021).

Acknowledgements

This study was supported by grants from the National Institutes of Health (HL149658, HL152176, HL149687, AR075867, DK132735 (A.D.) and T32 DK007044-41 (D.R.S.)). The funders had no role in study design, data collection and analysis, decision to publish or preparation of the manuscript.

Author contributions

S.R. and J.Q. performed majority of the experiments. B.T. and B.S. performed animal surgeries. F.M. and M.P. performed single-nuclear gene expression analysis. R.W. assisted in generation of the GPNMB KO animals and S.L. assisted in viral expression experiments. E.C. assisted with immunostaining. N.E.T., D.R.S., A.P., K.V.G. and P.L.S.M.G. performed experiments related to the identification of binding partners of GPNMB and A.J.L. performed analysis on the strength of

association of GPNMB in human heart failure. Y.Z. and J.W. constructed the plasmids. B.H. generated GPR39 KO mice. A.D. conceptualized the project, designed experiments, supervised data collection and analysis and wrote the paper.

Competing interests
The authors declare no competing interests.

Additional information
Extended data is available for this paper at https://doi.org/10.1038/s44161-024-00555-4.

Supplementary information The online version contains supplementary material available at https://doi.org/10.1038/s44161-024-00555-4.

Correspondence and requests for materials should be addressed to Arjun Deb.

Peer review information *Nature Cardiovascular Research* thanks Kory Lavine and the other, anonymous, reviewer(s) for their contribution to the peer review of this work.

[1]Division of Cardiology, Department of Medicine, David Geffen School of Medicine, University of California-Los Angeles, Los Angeles, CA, USA. [2]UCLA Cardiovascular Theme, David Geffen School of Medicine, University of California-Los Angeles, Los Angeles, CA, USA. [3]Department of Molecular, Cell and Developmental Biology, College of Letters and Sciences, University of California-Los Angeles, Los Angeles, CA, USA. [4]Eli & Edythe Broad Center of Regenerative Medicine and Stem Cell Research, University of California-Los Angeles, Los Angeles, CA, USA. [5]Molecular Biology Institute, University of California-Los Angeles, Los Angeles, CA, USA. [6]California Nanosystems Institute, University of California-Los Angeles, Los Angeles, CA, USA. [7]Department of Cellular and Molecular Medicine, University of California-San Diego, La Jolla, CA, USA. [8]Glycobiology Research and Training Center, University of California-San Diego, La Jolla, CA, USA. [9]Department of Cell and Development Biology, Feinberg School of Medicine, Northwestern University, Chicago, IL, USA. [10]Department of Biomedical Sciences, University of Copenhagen, Copenhagen, Denmark. [11]Department of Genetics, David Geffen School of Medicine, University of California-Los Angeles, Los Angeles, CA, USA. [12]These authors contributed equally: Sivakumar Ramadoss, Juan Qin.
✉e-mail: adeb@mednet.ucla.edu

https://doi.org/10.1038/s44161-024-00555-4

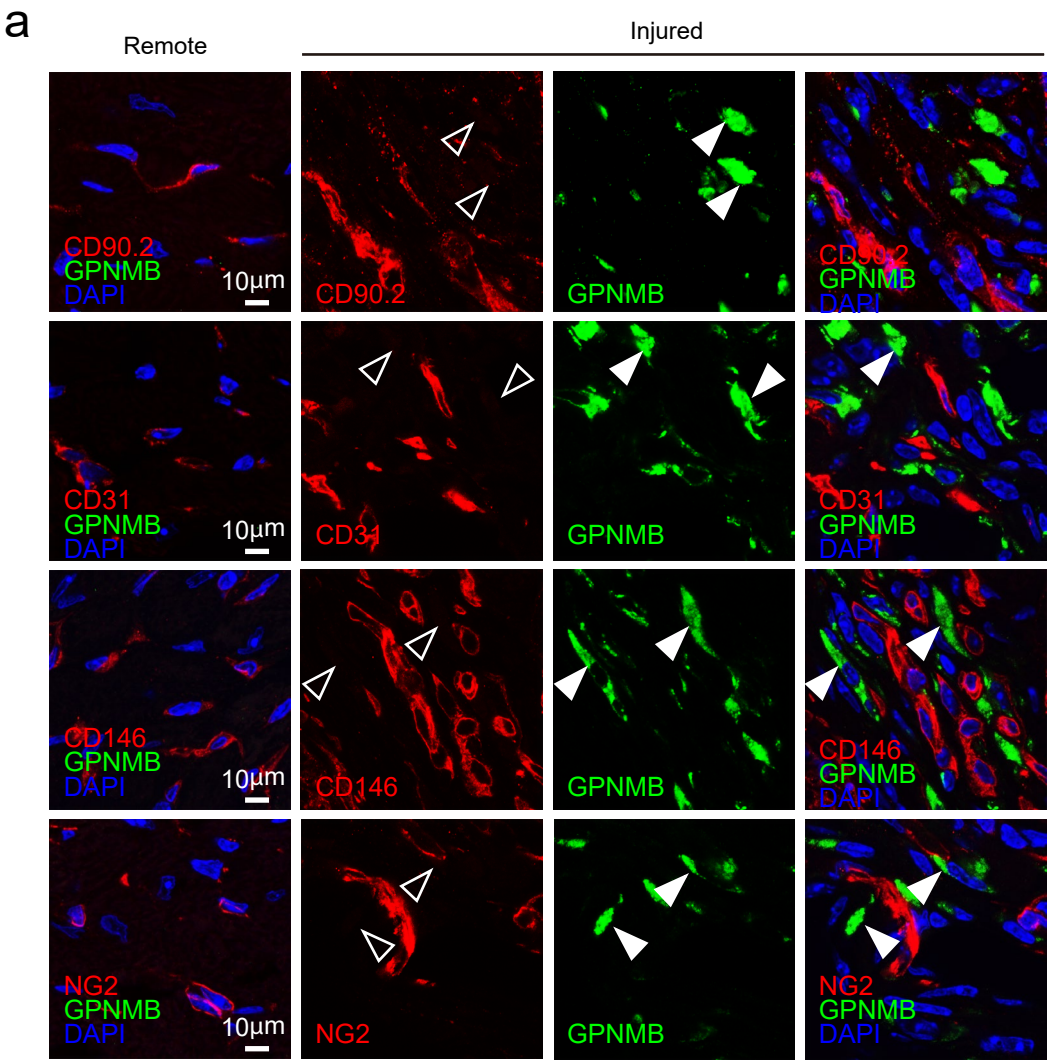

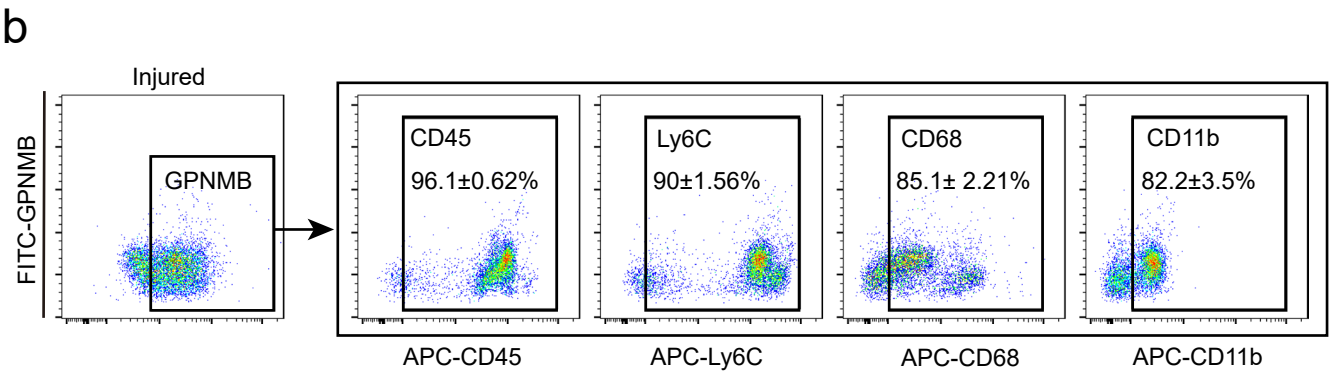

Extended Data Fig. 1 | GPNMB expression in the infarcted heart using immunofluorescent staining and flow cytometry. a, Immunofluorescent staining, and confocal microscopy of GPNMB expression in uninjured (remote) and injured regions of heart demonstrating that GPNMB (green, arrows) is not coexpressed with CD90.2, CD31, CD146 and NG2 markers (red, arrows) at Day 7 post infarction (Representative images, n=3 animals). **b**, Flow cytometry of nonmyocytes in the heart 7 days after MI demonstrating the expression of GPNMB in macrophages (CD45, Ly6C, CD68 and CD11b, n=5 animals). Data presented as mean±SEM.

https://doi.org/10.1038/s44161-024-00555-4

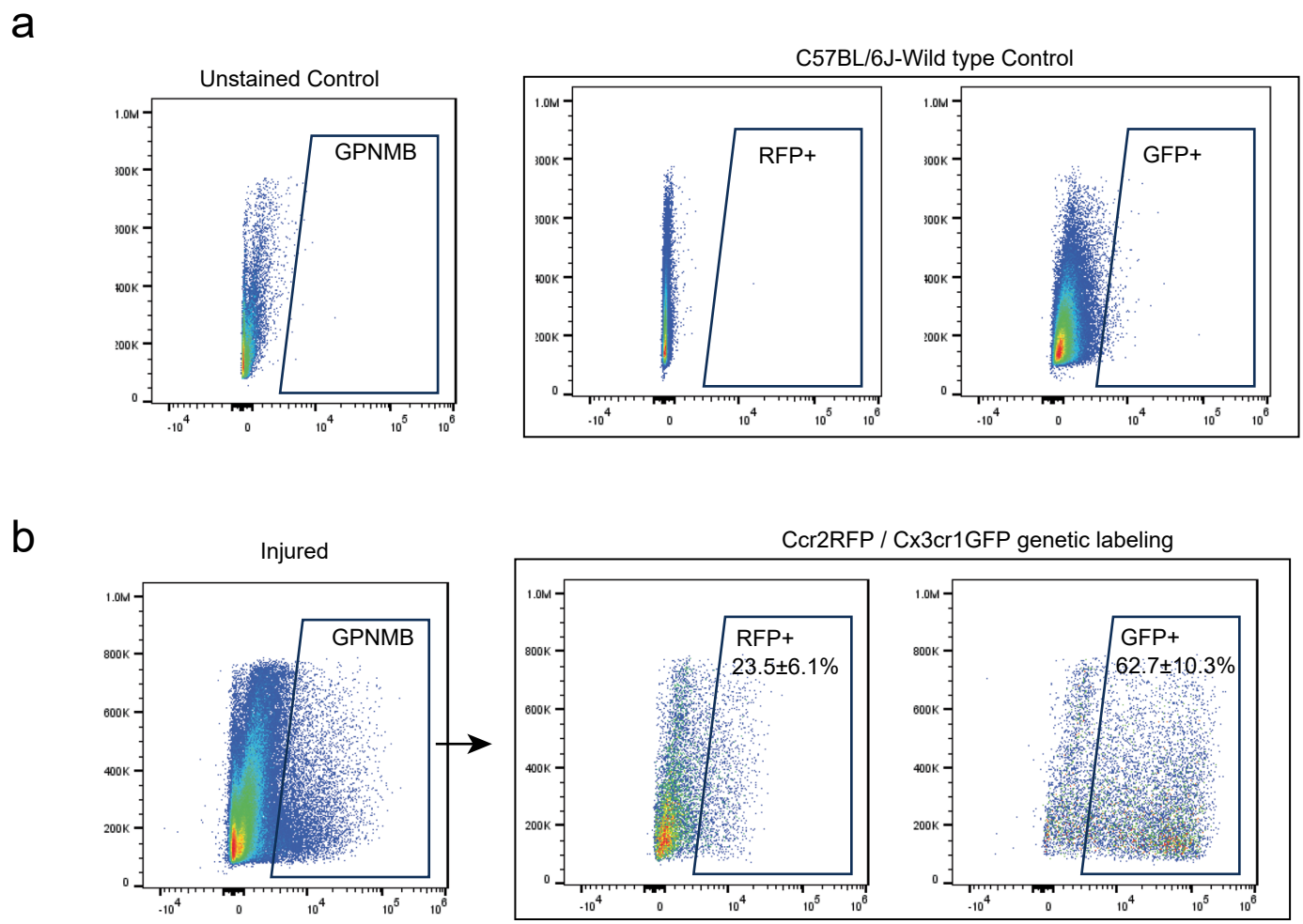

Extended Data Fig. 2 | Flow cytometry to demonstrate expression of RFP+ and GFP+ cells in infarcted hearts of Ccr2^{RFP}Cx3cr1^{GFP} mice. a, Flow cytometry gating controls on nonmyocytes isolated from wild-type mice (using unstained controls for GPNMB and gates for RFP and GFP). **b**, GPNMB expression in infarcted hearts of Ccr2^{RFP}Cx3cr1^{GFP} mice on day 7 following MI demonstrating GPNMB is predominantly expressed in the GFP and RFP positive cells (62.7±10% (GFP) and 23.5±6% (RFP), n=3 animals/group).

https://doi.org/10.1038/s44161-024-00555-4

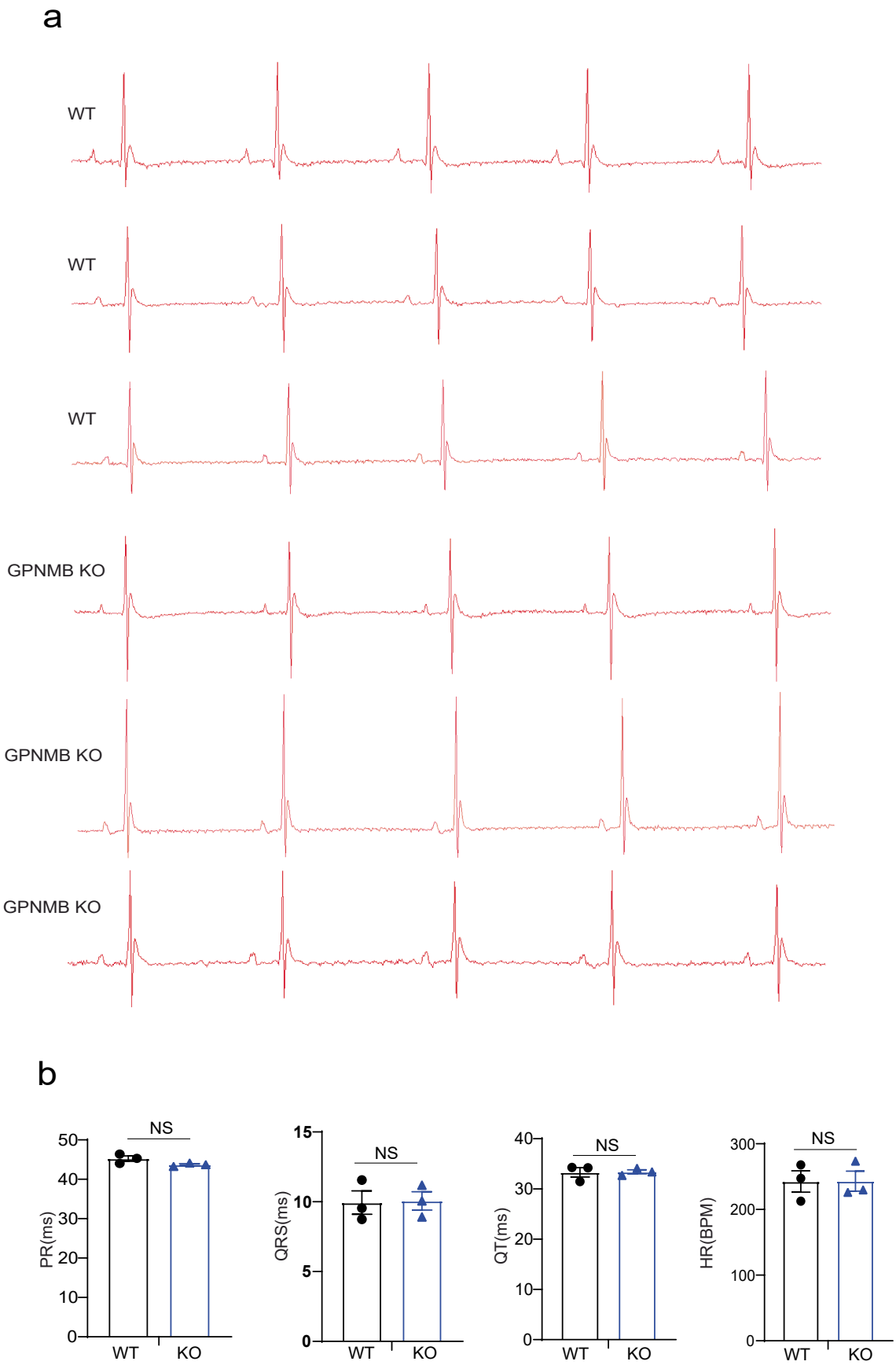

Extended Data Fig. 3 | Global depletion of GPNMB doesn't affect the electrical activation pattern. a, Surface ECG of age and sex matched WT and GPNMB KO animals demonstrating similar electrical activation patterns. **b**, ECG intervals showing PR, QRS, QT intervals and heart rate in WT and GPNMB KO animals (mean±SEM, n=3, Two-tailed Student's t-test, NS=Not significant).

https://doi.org/10.1038/s44161-024-00555-4

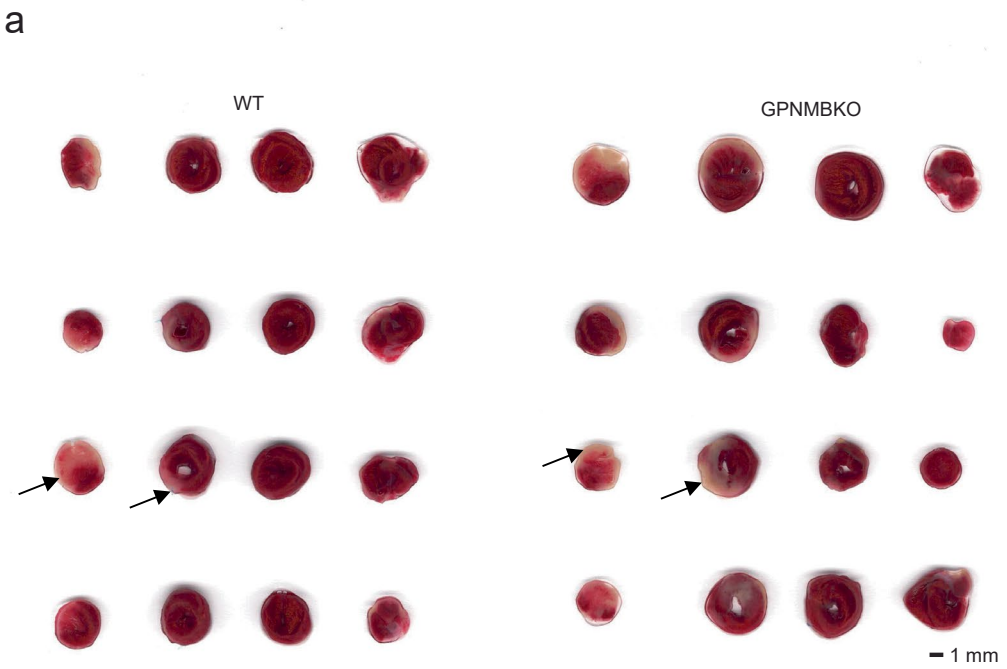

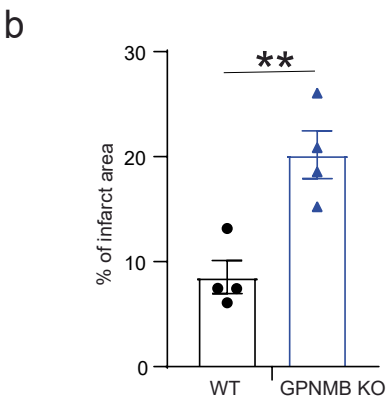

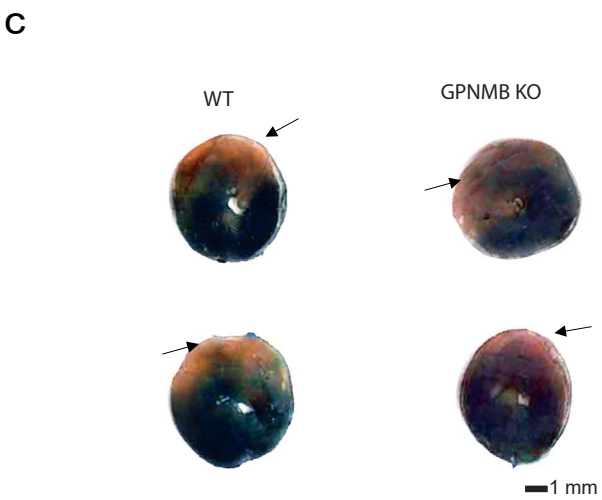

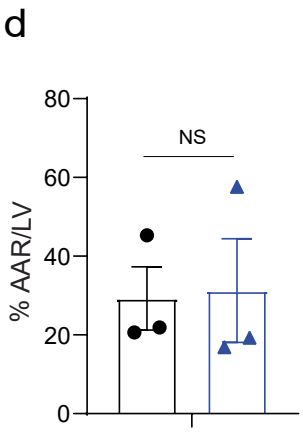

Extended Data Fig. 4 | See next page for caption.

https://doi.org/10.1038/s44161-024-00555-4

Extended Data Fig. 4 | GPNMB deficiency increases infarct size but did not affect the area at risk after MI. a, Images showing the transverse slices of Triphenyltetrazolium chloride (TTC) stained heart of wild-type and GPNMB KO mice on day 3 of myocardial injury. The red zone indicates viable heart tissue, and the white zone (arrows) represents non-viable infarct area. **b**, Relative % of infarct area in the hearts of WT and GPNMB KO mice on day 3 after myocardial injury (mean±SEM, n=4 animals, **p<0.0044 by two-tailed Student's *t*-test). **c**, Representative image showing the transverse slices of hearts of WT and GPNMB KO mice stained with Evans blue at 24hr after myocardial injury. The red zone (arrow) indicates area of risk and blue zone indicates non-risk area. **d**, Relative % of area at risk in the hearts of WT and GPNMB KO mice. (mean±SEM, n=3 animals, Two-tailed Student's t-test, NS=Not significant).

https://doi.org/10.1038/s44161-024-00555-4

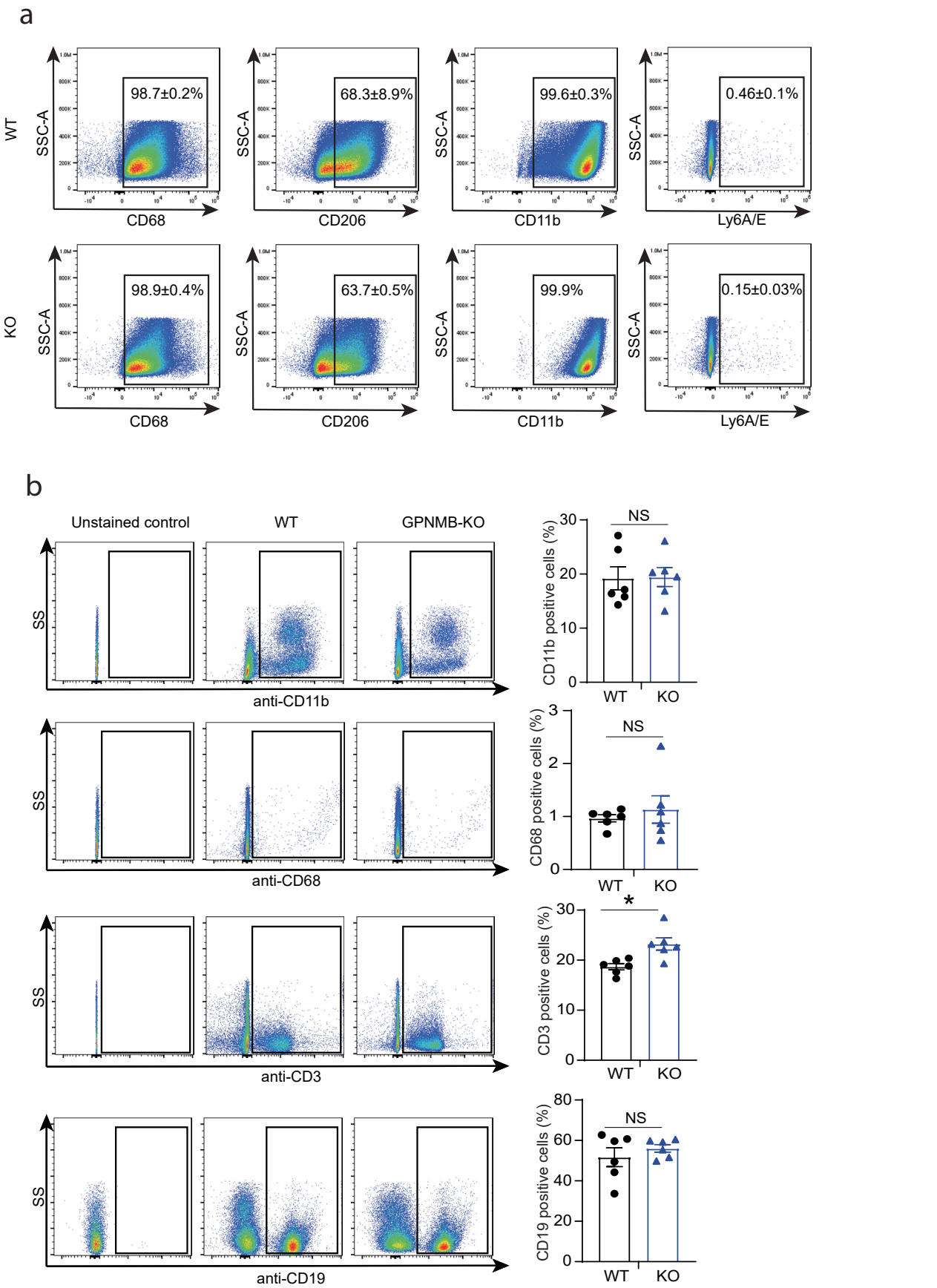

Extended Data Fig. 5 | See next page for caption.

https://doi.org/10.1038/s44161-024-00555-4

Extended Data Fig. 5 | Effects of GPNMB depletion on bone marrow macrophage and peripheral immune cell composition. a, Flow cytometry of bone marrow macrophages isolated from WT and GPNMB KO mice demonstrating the percentage of CD68, CD206, CD11b and Ly6A/E expressing cell population. **b**, Flow cytometry of peripheral immune cells isolated from WT and GPNMB KO animals demonstrating the percentage of CD11b, CD68, CD3 and CD19 expressing cells (mean±SEM, n=3 animals/group, * $p<0.016$ by Two-tailed Student's *t*-test, NS=Not significant).

https://doi.org/10.1038/s44161-024-00555-4

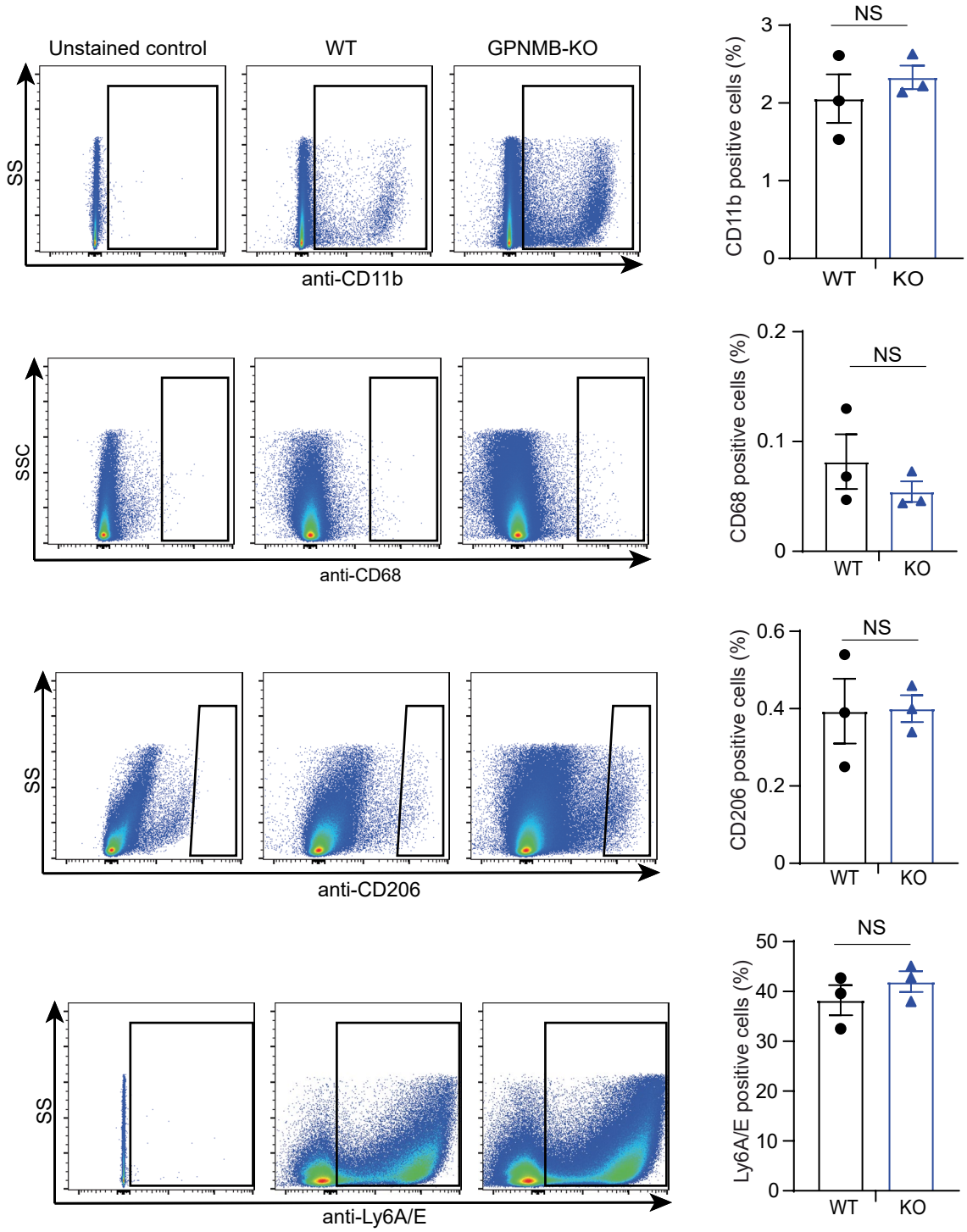

Extended Data Fig. 6 | Resident macrophage composition in hearts of WT and GPNMB KO animals. Flow cytometry of macrophages isolated from WT and GPNMB KO hearts demonstrating the percentage of CD11b, CD68, CD206, and Ly6A/E expressing cell population. (mean±SEM, n=3 animals/group, Two-tailed Student's *t* test, NS=Not significant).

https://doi.org/10.1038/s44161-024-00555-4

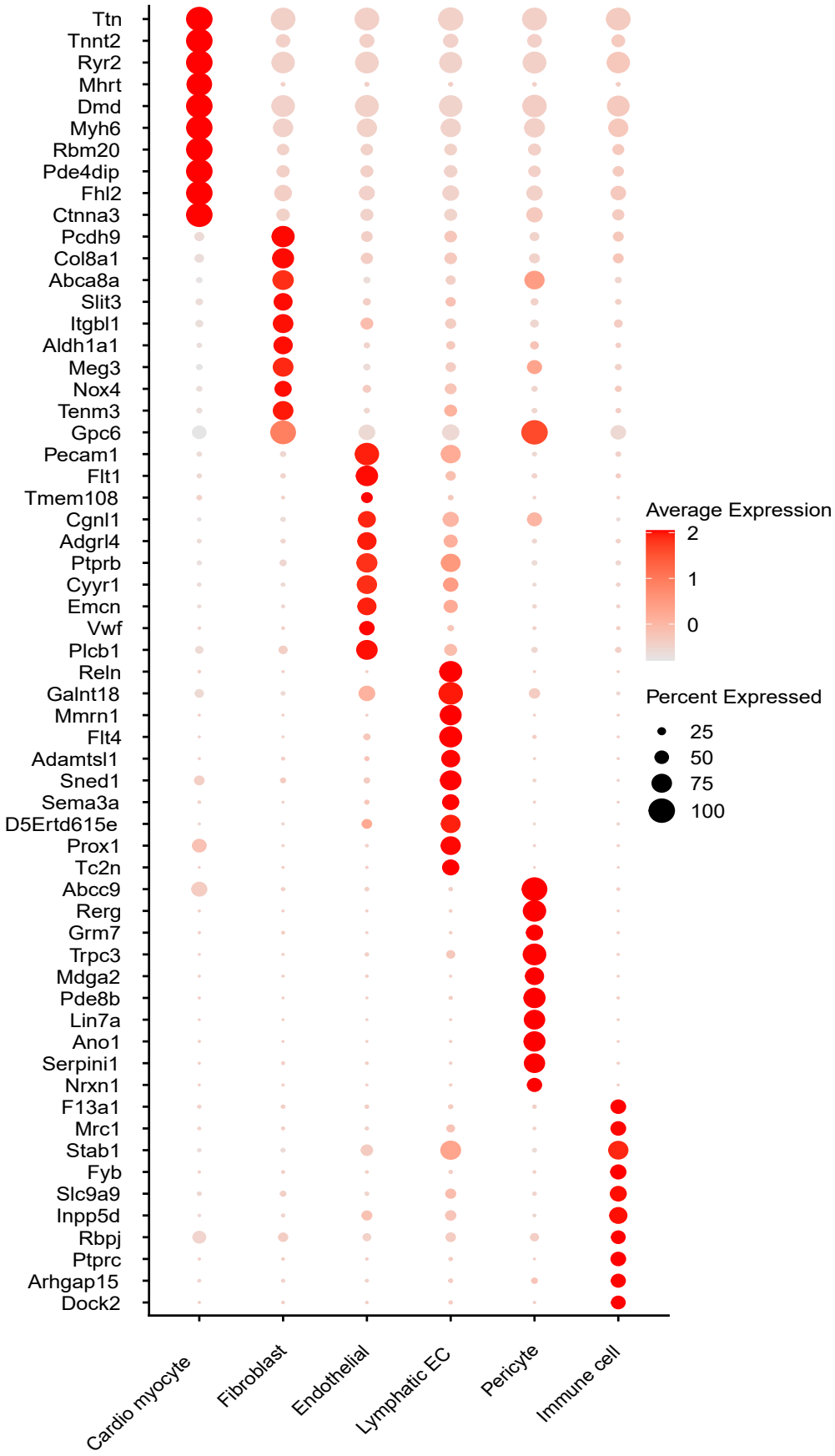

Extended Data Fig. 7 | Canonical genes used to identify cell population in the heart following single nuclear seq. Dot plot demonstrating clusters of genes used to identify cardiomyocyte and nonmyocyte cell populations in snRNA-seq of the heart at 7 days after MI (n=4 animals).

https://doi.org/10.1038/s44161-024-00555-4

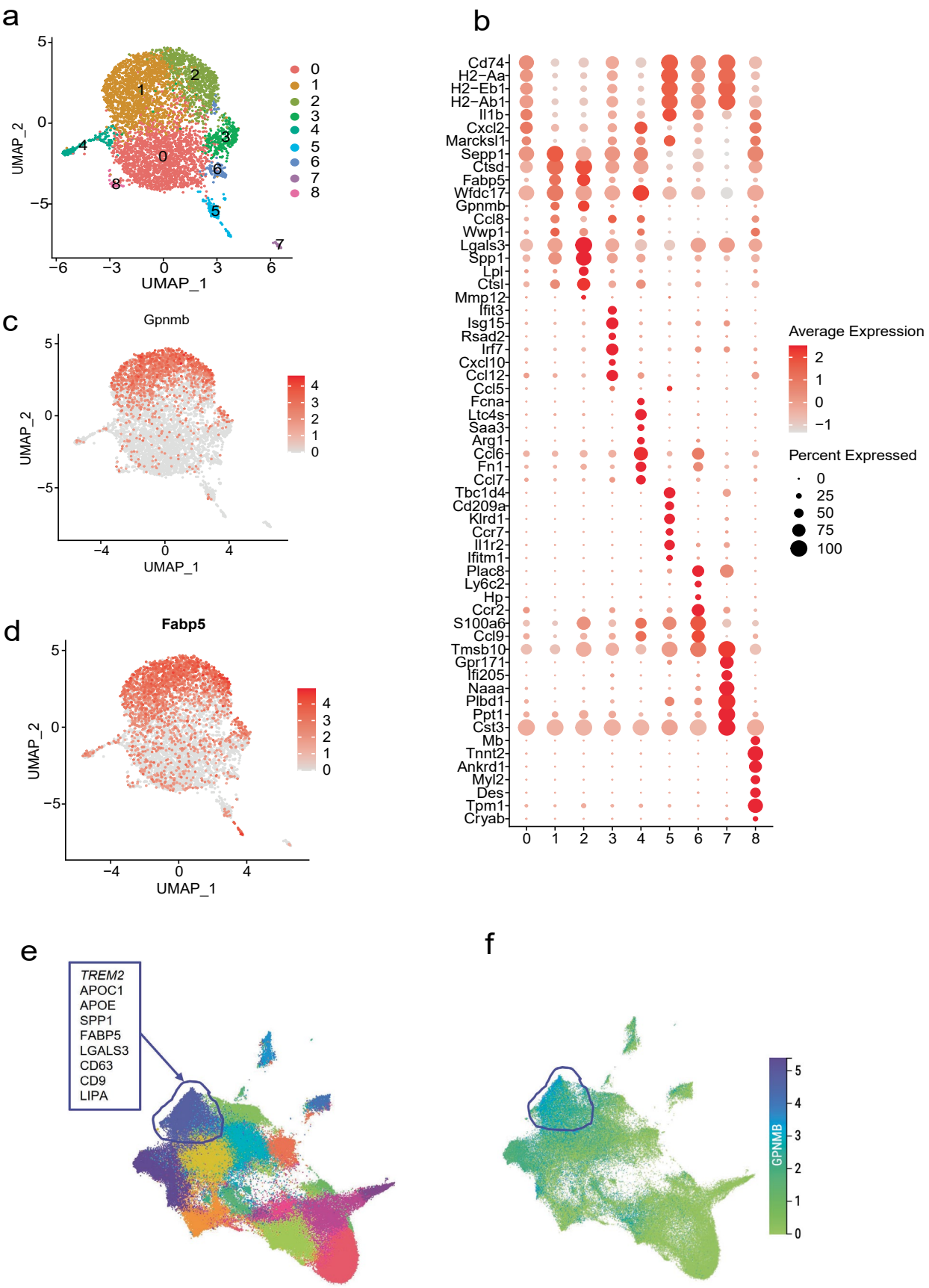

Extended Data Fig. 8 | See next page for caption.

https://doi.org/10.1038/s44161-024-00555-4

Extended Data Fig. 8 | GPNMB is predominantly expressed in specific subclusters of macrophages in the infarcted heart. a, UMAP of myeloid subtype clusters in the injured murine heart on day 7 after MI. **b**, Cluster markers of myeloid subtype populations in the injured heart on day 7 after MI. **c**, UMAP showing GPNMB expression in specific subclusters (1&2). **d**, UMAP showing FABP5 expression in specific subclusters (1&2). **e, f**, UMAP showing the robust expression of GPNMB in TREM2 macrophage cluster of macrophage/monocyte atlas of healthy and pathologic tissues in humans (Mudler et al., 2021).

https://doi.org/10.1038/s44161-024-00555-4

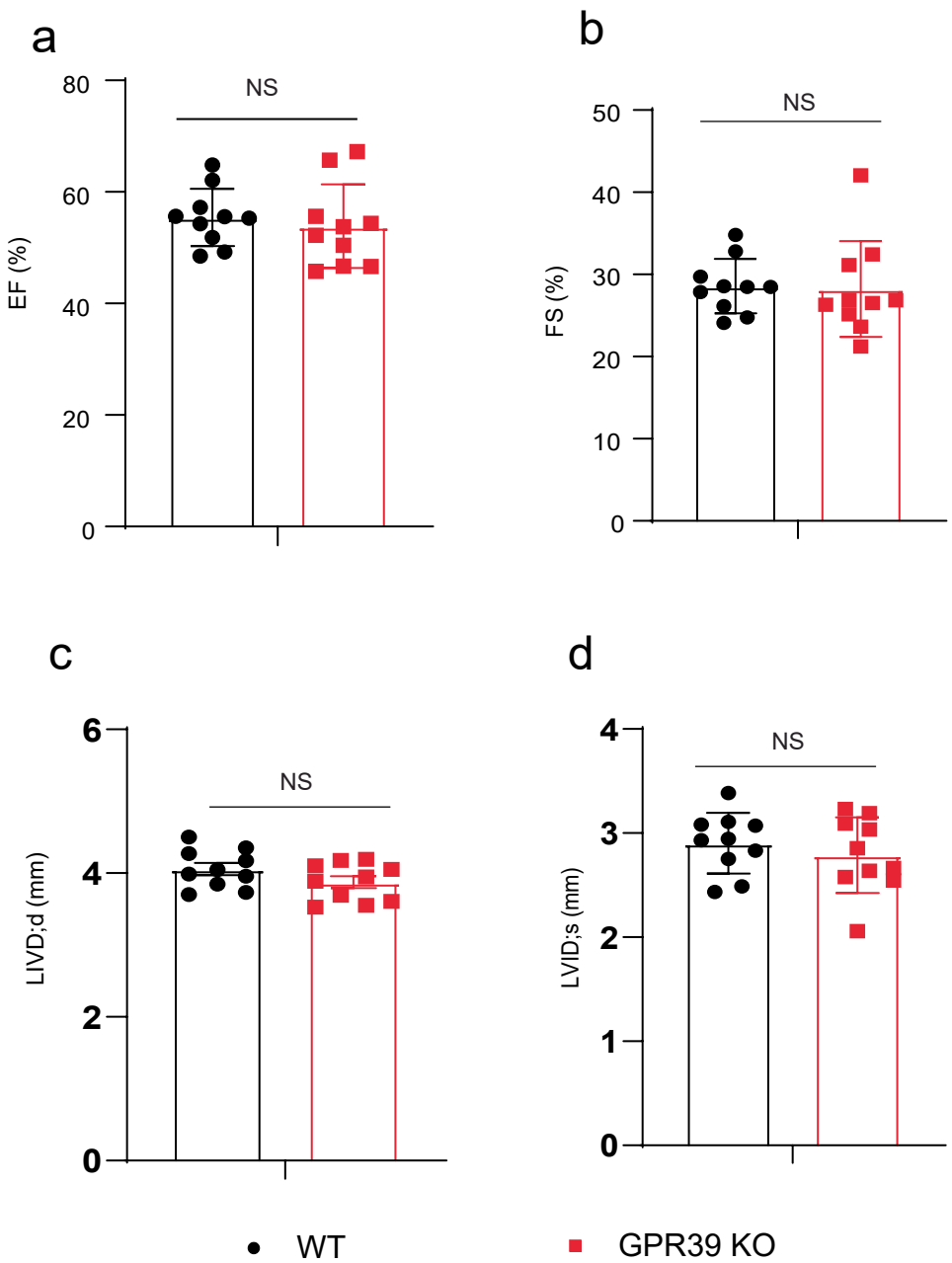

Extended Data Fig. 9 | Genetic deletion of GPR39 did not influence cardiac function in normal conditions. (**a**) Ejection fraction, (**b**) Fractional shortening and LV chamber size (LVID) in systole (**c**), and diastole (**d**) (Data presented as mean±SEM, n=10 animals/group, Two-tailed Student's *t*-test, NS=Not significant).

https://doi.org/10.1038/s44161-024-00555-4

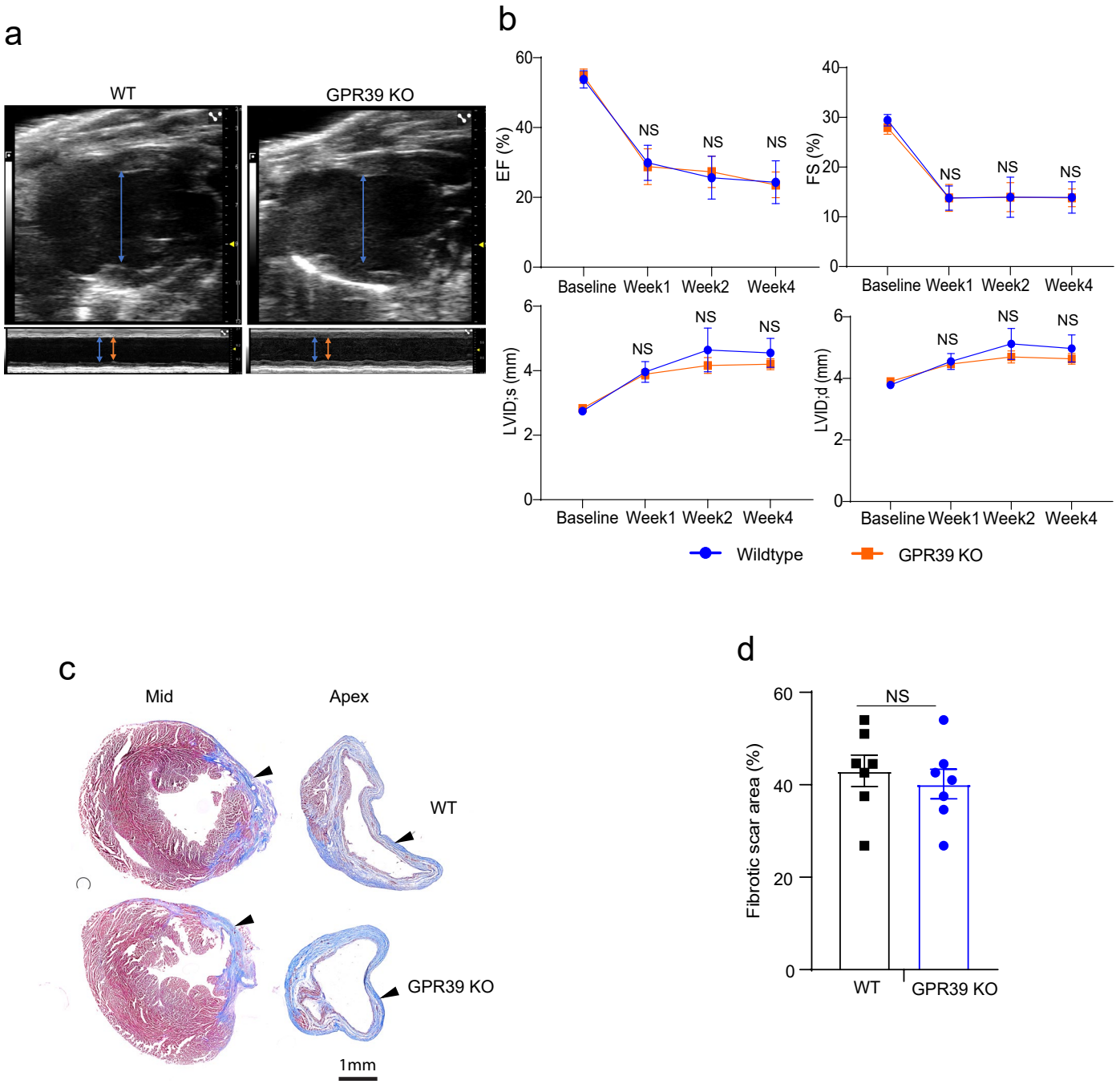

Extended Data Fig. 10 | Genetic deletion of GPR39 did not affect post-MI cardiac function. a, B-mode and M-mode echocardiogram demonstrating diminished contractile function with chamber dilatation at 4 weeks of cardiac injury in WT and GPR39 KO animals (orange arrows, diastole; blue arrows, systole). **b**, EF and FS and LV chamber size (LVID) in systole and diastole over 4 weeks after cardiac injury in WT and GPR39 KO animals (Baseline n=10, WT week 1 n=9, week2 n=7, Week4 n=7; GPR39 KO week 1 n=9, week2 n=9, Week4 n=7. Two-way ANOVA with Tukey's multiple comparison). Note cardiac function at baseline is not different between WT and GPR39 KO animals. **c**, Masson trichrome staining demonstrating the scar in the apex and mid-ventricle (arrows). **d**, Quantitation of fibrotic scar area in the apex and mid-ventricle. (Data presented as mean±SEM. n=7 animals, Two-tailed Student's *t* test, NS=Not significant).

nature portfolio

Corresponding author(s): Arjun Deb

Last updated by author(s): 10/09/2024

Reporting Summary

Nature Portfolio wishes to improve the reproducibility of the work that we publish. This form provides structure for consistency and transparency in reporting. For further information on Nature Portfolio policies, see our Editorial Policies and the Editorial Policy Checklist.

Statistics

For all statistical analyses, confirm that the following items are present in the figure legend, table legend, main text, or Methods section.

n/a	Confirmed
☐	☒ The exact sample size (*n*) for each experimental group/condition, given as a discrete number and unit of measurement
☐	☒ A statement on whether measurements were taken from distinct samples or whether the same sample was measured repeatedly
☐	☒ The statistical test(s) used AND whether they are one- or two-sided *Only common tests should be described solely by name; describe more complex techniques in the Methods section.*
☐	☒ A description of all covariates tested
☐	☒ A description of any assumptions or corrections, such as tests of normality and adjustment for multiple comparisons
☐	☒ A full description of the statistical parameters including central tendency (e.g. means) or other basic estimates (e.g. regression coefficient) AND variation (e.g. standard deviation) or associated estimates of uncertainty (e.g. confidence intervals)
☐	☒ For null hypothesis testing, the test statistic (e.g. *F*, *t*, *r*) with confidence intervals, effect sizes, degrees of freedom and *P* value noted *Give P values as exact values whenever suitable.*
☒	☐ For Bayesian analysis, information on the choice of priors and Markov chain Monte Carlo settings
☒	☐ For hierarchical and complex designs, identification of the appropriate level for tests and full reporting of outcomes
☒	☐ Estimates of effect sizes (e.g. Cohen's *d*, Pearson's *r*), indicating how they were calculated

Our web collection on statistics for biologists contains articles on many of the points above.

Software and code

Policy information about availability of computer code

Data collection	Echocardiographic imaging and data was collected using a Vevo 3100 Imaging System with a 30 MHz linear probe (Visualsonics, Canada). Flow cytometry was performed using LSRII IMED (BD Biosciences) or sorted on FACS Aria II (BD Biosciences).
Data analysis	All the software used for data analysis were described in the manuscript .Image J version 1.49 used for image analysis. Prism 7.02 was used for statistical analysis. FlowJo 10.4 used for flow cytometry data analysis. Echo data analysed using Vevo3100 software.

For manuscripts utilizing custom algorithms or software that are central to the research but not yet described in published literature, software must be made available to editors and reviewers. We strongly encourage code deposition in a community repository (e.g. GitHub). See the Nature Portfolio guidelines for submitting code & software for further information.

Data

Policy information about availability of data

All manuscripts must include a data availability statement. This statement should provide the following information, where applicable:

- Accession codes, unique identifiers, or web links for publicly available datasets
- A description of any restrictions on data availability
- For clinical datasets or third party data, please ensure that the statement adheres to our policy

The snRNA-seq data generated for this study were deposited in the Gene Expression Omnibus under accession numbers GSE235434 and GSE277086.

Research involving human participants, their data, or biological material

Policy information about studies with human participants or human data. See also policy information about sex, gender (identity/presentation), and sexual orientation and race, ethnicity and racism.

Reporting on sex and gender	Not applicable
Reporting on race, ethnicity, or other socially relevant groupings	Not applicable
Population characteristics	Not applicable
Recruitment	Not applicable
Ethics oversight	Not applicable

Note that full information on the approval of the study protocol must also be provided in the manuscript.

Field-specific reporting

Please select the one below that is the best fit for your research. If you are not sure, read the appropriate sections before making your selection.

☒ Life sciences ☐ Behavioural & social sciences ☐ Ecological, evolutionary & environmental sciences

For a reference copy of the document with all sections, see nature.com/documents/nr-reporting-summary-flat.pdf

Life sciences study design

All studies must disclose on these points even when the disclosure is negative.

Sample size	Sample size were chosen based on our previous publications and guide lines . https://pubmed.ncbi.nlm.nih.gov/32621799/ https://pubmed.ncbi.nlm.nih.gov/34813507/
Data exclusions	No data excluded
Replication	3-5 replications and most of the time it is successful
Randomization	There is no randomization involved because we did not use any drug to treat the conditions.
Blinding	Since we did not conduct any drug testing studies, it is not applicable for this work.

Reporting for specific materials, systems and methods

We require information from authors about some types of materials, experimental systems and methods used in many studies. Here, indicate whether each material, system or method listed is relevant to your study. If you are not sure if a list item applies to your research, read the appropriate section before selecting a response.

Materials & experimental systems

n/a	Involved in the study
☐	☒ Antibodies
☐	☒ Eukaryotic cell lines
☒	☐ Palaeontology and archaeology
☐	☒ Animals and other organisms
☐	☐ Clinical data
☒	☐ Dual use research of concern
☒	☐ Plants

Methods

n/a	Involved in the study
☒	☐ ChIP-seq
☐	☒ Flow cytometry
☒	☐ MRI-based neuroimaging

Antibodies

Antibodies used	Rabbit anti-GPR39 (1;1000, Novas Cat. No. NLS139, Lot A-6); rabbit anti-GPNMB (1:200 dilution, Cell Signaling, 90205); rat anti-CD45 (1:100 dilution, Millipore, 051416); rabbit anti-CD68 (1:100 dilution, Abcam, ab125212); rat anti-CD11b (1:100 dilution, Abcam, ab8878); rat anti-F4/80 (1:100 dilution, Invitrogen, MA191124); rat anti-CD31 (1:200 dilution, Abcam, ab7388); rabbit anti-CD146

(1:200 dilution, Abcam, ab75769); rabbit anti-NG2 (1:200 dilution, Millipore Sigma, AB5320); rat anti-CD90.2 (1:50 dilution, BD Biosciences, 566082); rabbit anti-cardiac troponin I (1:100 dilution, Abcam, ab47003); Alexa Fluor 594 conjugated WGA (5μgml−1, Invitrogen, W11262). APC-conjugated anti-CD45 (1:100 dilution, BioLegend, 103111); APC-conjugated anti-CD68 (1:100 dilution, BioLegend, 137007); APC-conjugated anti-CD11b (1:100 dilution, Invitrogen, 13011281); Alexa Fluor anti-GPNMB (1:100 dilution, Abcam, Ab284639); Brilliant Violet anti-CD11b (1:100 dilution, BioLegend, 101235); PE anti-CD3 (1;100 dilution, BioLegend, 100205); FITC anti-CD19 (1:100 dilution, BioLegend 101505); FITC-anti-Ly-6A/E (1:100 dilution, Thermo Fisher Scientific, 11-5981-82); Alexa Flour anti-CD206 (1:100 dilution, Thermo Fisher Scientific, 53-2061-82); APC-conjugated anti-Ly-6C (1:100 dilution, BioLegend,128015); and eFluor anti-GPNMB (1:100 dilution, Invitrogen, 50-5708-82); rabbit anti-p-AKT (Ser 473) (1:2,000 dilution, Cell Signaling, 4060), rabbit anti-p-ERK (1:1,500 dilution, Cell Signaling, 4695), rabbit anti-AKT (1:2,000 dilution, Cell Signaling, 4691), mouse anti-ERK (1:1,000 dilution, Sata Cruz, 514302), goat anti-GPNMB (1:1,000 dilution, R&D Systems, AF2330), rabbit anti-GAPDH (1:2,000 dilution, Cell Signaling, 2118), mouse anti-Flag (1:1,000 dilution, Proteintech, 66008-3Ig); rabbit anti-His-tag (1:1,000 dilution, Proteintech, 10001-0-AP).

Validation

Each antibody was validated using positive and negative control samples. We validated all the above mentioned antibodies work for the mouse tissues and cells and cells obtained form rats, wherever applicable.

Eukaryotic cell lines

Policy information about cell lines and Sex and Gender in Research

Cell line source(s)	HEK293 cells were obtained from ATCC (CRL 1573). Cardiac fibroblast and neonatal rat ventricular myocytes were isolated and used.
Authentication	HEK293 cells obtained from ATCC were authenticated by several studies
Mycoplasma contamination	The cells maintained in normocin to prevent mycoplasma contamination and often tested negative for myoplasma.
Commonly misidentified lines (See ICLAC register)	We did not use any commonly misidentified cells or cell lines.

Animals and other research organisms

Policy information about studies involving animals; ARRIVE guidelines recommended for reporting animal research, and Sex and Gender in Research

Laboratory animals	Wildtype, GPNMB KO and GPR39 KO mouse of C57BL/6J background were used for this study. Both the genders at the age of 8-12 weeks old were used. Neonatal Rat Ventricular Myocyted were isolated from 1 day old Sprague-Dawley rat pups. The animals were housed in the clean cages with standard condition at vivarium (ambient temperature, 40-60% humudity, 12light/12 dark schdule)
Wild animals	No wild animals used in this study
Reporting on sex	We used both the gender of animals for this study. Therefore, there is no gender specific data generated.
Field-collected samples	No field collected samples used in this study
Ethics oversight	Animal Research Committee UCLA

Note that full information on the approval of the study protocol must also be provided in the manuscript.

Clinical data

Policy information about clinical studies

All manuscripts should comply with the ICMJE guidelines for publication of clinical research and a completed CONSORT checklist must be included with all submissions.

Clinical trial registration	No clinical data collected in this study
Study protocol	Not applicable
Data collection	Not applicable
Outcomes	Not applicable

Plants

Seed stocks	No plant used in this study
Novel plant genotypes	Not applicable
Authentication	Not applicable

Flow Cytometry

Plots

Confirm that:

☒ The axis labels state the marker and fluorochrome used (e.g. CD4-FITC).

☒ The axis scales are clearly visible. Include numbers along axes only for bottom left plot of group (a 'group' is an analysis of identical markers).

☒ All plots are contour plots with outliers or pseudocolor plots.

☒ A numerical value for number of cells or percentage (with statistics) is provided.

Methodology

Sample preparation	Cells will be isolated from heart by enzymatic digestion
Instrument	LSRII IMED (BD Biosciences)
Software	Flowjo
Cell population abundance	90%
Gating strategy	Flow core determined the gating strategy based on the unstained samples

☒ Tick this box to confirm that a figure exemplifying the gating strategy is provided in the Supplementary Information.